

The multi-configurational time-dependent Hartree approach in optimized second quantization: imaginary time propagation and particle number conservation

Thomas Weike^{1, a)} and Uwe Manthe^{1, b)}

Theoretische Chemie, Fakultät für Chemie, Universität Bielefeld, Universitätsstr. 25, D-33615 Bielefeld, Germany

(Dated: December 3, 2019)

The multi-layer multi-configurational time-dependent Hartree (MCTDH) in optimized second quantization representation (oSQR) approach combines the tensor contraction scheme of the multi-layer MCTDH approach with the use of an optimized time-dependent orbital basis. Extending the original work on the subject [Manthe, Weike, *J. Chem. Phys.* 146, 064117 (2017)], here MCTDH-oSQR propagation in imaginary time and properties related to particle number conservation are studied. Difference between the orbital equation of motion in real and imaginary time are highlighted and a new gauge operator which facilitates efficient imaginary time propagation is introduced. Studying Bose-Hubbard models, particle number conservation in MCTDH-oSQR calculations is investigated in detail. Interesting properties of the single-particle functions used in the multi-layer MCTDH representation are identified. Based on these results, a tensor contraction scheme which explicitly utilizes particle number conservation is suggested.

I. INTRODUCTION

The (multi-layer) multi-configurational time-dependent Hartree (MCTDH) approach¹⁻⁴ facilitates accurate high-dimensional quantum dynamics calculations. It is used by many research groups to study a variety of systems.⁵⁻²⁴ Benchmark applications studied bimolecular reactions²⁵⁻³⁸, proton transfer³⁹⁻⁴⁴, and large amplitude motion⁴⁵⁻⁴⁹ for molecular systems including six to nine atoms on accurate ab initio potential energy surfaces. MCTDH simulations based on model Hamiltonians describing non-adiabatic dynamics⁵⁰⁻⁵² or electron and proton transfer processes in condensed matter⁵³⁻⁵⁷ considered significantly larger numbers of degrees of freedom ranging up to 10^3 - 10^4 .

The MCTDH approach was originally introduced to describe the quantum dynamics of molecular systems. The molecular wave function was specified as a function depending on geometry-dependent coordinates and indistinguishable particle symmetries were not explicitly considered. Subsequently MCTDH-type approaches designed for the efficient description of bosonic and fermionic systems have been introduced⁵⁸⁻⁶⁴ and applied in different areas⁶⁵⁻¹⁰⁸. These approaches are often formulated in second quantization. Two different strategies have mainly been utilized in this context.

One family of approaches^{58-63,102}, collectively denoted as MCTDH-X approaches in the following, employ time-dependent orbitals and a particle-number based truncation of the (time-dependent) configuration space. The active space is typically restricted to include all configurations with a specific number of particles. Consequently, the active space employed in MCTDH-X approaches is

invariant under time-dependent unitary transformation of the orbitals. The numerical efficiency of the approach relies on the combination of the particle-number based truncation scheme and the use of optimized time-dependent orbitals.

The multi-layer MCTDH approach in second quantization representation (ML-MCTDH-SQR)⁶⁴ employs a different strategy. Here the numerical efficiency is achieved by utilizing tensor contraction instead of truncation. Wang and Thoss introduced the approach using a primitive time-independent orbital basis. The ML-MCTDH-SQR approach is designed to treat general Hamiltonians and does not consider particle number-based properties explicitly.

Recently the multi-layer MCTDH in optimized second quantization representation ML-MCTDH-oSQR which includes features of the ML-MCTDH-SQR approach and the MCTDH-X approaches has been introduced.¹⁰⁹ The ML-MCTDH-oSQR approach combines the use of optimized time-dependent orbitals with a ML-MCTDH-type tensor contraction scheme. In the ML-MCTDH-oSQR scheme the invariance with respect to time-dependent unitary transformations of the orbital basis, which is a typical feature in other MCTDH-type approaches, is absent. These unitary transformations give rise to gauge operators appearing in the MCTDH equations of motion. While the choice of these gauge operators does not affect the convergence properties in other MCTDH-type approaches, it is an important issue in the ML-MCTDH-oSQR approach. The choice of a natural orbital basis was suggested in Ref. 109 and the corresponding gauge operators were derived. A numerical test for the spin-boson-model was presented to illustrate the efficiency of the approach.

The present work explores aspects of the ML-MCTDH-oSQR approach which have not been addressed in Ref. 109. In this original work only propagation in real time

^{a)} Electronic mail: t.weike@uni-bielefeld.de

^{b)} Electronic mail: uwe.manthe@uni-bielefeld.de

was considered. However, the presence of relevant gauge operators results in significant differences between real and imaginary time propagation in the ML-MCTDH-oSQR approach. While gauge operators are hermitian in the real time equations of motion, they are anti-hermitian in the imaginary time ones. This difference affects the choice of efficient gauge operators. A new type of gauge operators more suitable for imaginary time propagations is introduced and tested in the present work.

Particle number conservation is another important aspect not considered in previous work on the ML-MCTDH-SQR and ML-MCTDH-oSQR approaches. These approaches are formulated in Fock space and thus can contain states with all possible particle numbers. Appropriate initial conditions can in principle be used to obtain results for a specific particle number. While this strategy tends to work well in real time dynamics, the exponential increase of small wave function components can result in unphysical results in imaginary time propagation. Practical solutions to this problem are investigated in this work.

The present article is organized as follows. After a brief review of the MCTDH-oSQR approach for real time propagation in section II, the equations of motions for the imaginary time are discussed in Sec. III. In Sec. IV, different gauges are discussed and a new gauge which can be efficiently employed in imaginary time propagation is introduced. Constraining operators which guarantee particle number conservation during propagation in imaginary time are described in Sec. V. The different aspects are illustrated by numerical examples studying Bose-Hubbard models in Sec. VI. An important result of the numerical study, the conservation of local particle numbers at all layers of wavefunction representation, is discussed in more detail in Sec. VII. There also an efficient tensor contraction scheme utilizing the particle number conservation to reduce the numerical effort is suggested. Finally, concluding remarks are given in Sec. VIII.

II. MCTDH-oSQR

In the MCTDH-oSQR approach¹⁰⁹ the wave function is represented in a basis of configurations,

$$|\Psi\rangle = \sum_{i_1} \dots \sum_{i_f} A_{i_1 \dots i_f}(t) |\Phi_{i_1 \dots i_f}(t)\rangle. \quad (1)$$

These configurations are direct products of powers of f time-dependent creation operators acting on the vacuum state:

$$|\Phi_{i_1 \dots i_f}(t)\rangle = \frac{(\hat{b}_1^\dagger(t))^{i_1}}{\sqrt{i_1!}} \dots \frac{(\hat{b}_f^\dagger(t))^{i_f}}{\sqrt{i_f!}} |0\rangle. \quad (2)$$

The f time-dependent creation operators \hat{b}_μ^\dagger are represented as linear combinations of F time-independent cre-

ation operators \hat{a}_k^\dagger :

$$\hat{b}_\mu^\dagger(t) = \sum_{k=1}^F c_{\mu k}(t) \hat{a}_k^\dagger. \quad (3)$$

The coefficients $c_{\mu k}$ (called orbitals) satisfy the orthonormality relation

$$\sum_{k=1}^F c_{\mu k}^*(t) c_{\nu k}(t) = \delta_{\mu\nu} \quad (4)$$

and thus obey

$$\sum_{k=1}^F c_{\mu k}^*(t) \frac{dc_{\nu k}}{dt} = - \sum_{k=1}^F \frac{dc_{\mu k}^*}{dt} c_{\nu k}(t). \quad (5)$$

The equations of motions for $A_{i_1 \dots i_f}(t)$ and $c_{\mu k}(t)$ are derived employing the Dirac Frenkel variational principle¹⁰⁹

$$\left\langle \delta\Psi \left| i \frac{d}{dt} - \hat{H} \right| \Psi \right\rangle. \quad (6)$$

The orthonormality of the coefficients $c_{\nu k}$ is enforced by the constraint that

$$h_{\mu\nu} = \sum_{k=1}^F c_{\mu k}^* i \frac{dc_{\nu k}}{dt} \quad (7)$$

is an hermitian matrix. This constraint corresponds to the gauge condition in the usual MCTDH formalism. Therefore the matrix $h_{\mu\nu}$ will be called 'gauge' matrix despite the fact that it does not correspond to a true gauge invariance in the present context.¹⁰⁹

The resulting equation of motion for the tensor $A_{i_1 \dots i_f}(t)$ is

$$i \frac{dA_{i_1 \dots i_f}}{dt} = \left\langle \Phi_{i_1 \dots i_f} \left| \hat{H} - \sum_{\mu, \nu=1}^f \hat{b}_\nu^\dagger h_{\nu\mu} \hat{b}_\mu \right| \Psi \right\rangle. \quad (8)$$

This equation shows an analogous structure to the standard MCTDH equation of motion for the coefficient tensor. The MCTDH-oSQR approach can thus straightforwardly be generalized to a multi-layer MCTDH-oSQR scheme. The equations of motion of the orbitals $c_{\mu k}(t)$ read

$$i \frac{dc_{\mu k}}{dt} = \sum_{\nu=1}^f h_{\mu\nu} c_{\nu k} + \sum_{l=1}^F \left(\delta_{kl} - \sum_{\nu=1}^f c_{\nu k} c_{\nu l}^* \right) \cdot \sum_{\lambda=1}^f \rho_{\mu\lambda}^{-1} \left\langle \Psi \left| \hat{b}_\lambda^\dagger \left[\hat{a}_l, \hat{H} \right]_{\hat{a}_i = \sum_{\kappa=1}^f c_{\kappa i} \hat{b}_\kappa} \right| \Psi \right\rangle \quad (9)$$

where

$$\rho_{\mu\lambda} = \left\langle \Psi \left| \hat{b}_\mu^\dagger \hat{b}_\lambda \right| \Psi \right\rangle. \quad (10)$$

The Hamiltonian H appearing in Eq. (9) is typically written employing the operators a_i and a_i^\dagger in normal ordering to facilitate an efficient evaluation of the expectation value $\langle \Psi | \hat{b}_\lambda^\dagger [\hat{a}_l, \hat{H}]_{\hat{a}_i = \sum_{\kappa=1}^f c_{\kappa i} \hat{b}_\kappa} | \Psi \rangle$. The subscript $\hat{a}_i = \sum_{\kappa=1}^f c_{\kappa i} \hat{b}_\kappa$ indicates that all time-independent operators \hat{a}_i and \hat{a}_i^\dagger are replaced by time-dependent operators \hat{b}_κ and \hat{b}_κ^\dagger after evaluation of the commutator $[\hat{a}_l, \hat{H}]$.

III. EQUATIONS OF MOTION IN IMAGINARY TIME

Considering MCTDH-oSQR propagation in imaginary time, $\tau = it$, the ansatz for the wave function analogously reads

$$|\Psi\rangle = \sum_{i_1} \dots \sum_{i_f} A_{i_1 \dots i_f}(\tau) |\Phi_{i_1 \dots i_f}(\tau)\rangle, \quad (11)$$

$$|\Phi_{i_1 \dots i_f}(\tau)\rangle = \frac{(\hat{b}_1^\dagger(\tau))^{i_1}}{\sqrt{i_1!}} \dots \frac{(\hat{b}_f^\dagger(\tau))^{i_f}}{\sqrt{i_f!}} |0\rangle, \quad (12)$$

$$\hat{b}_\mu^\dagger(\tau) = \sum_{k=1}^F c_{\mu k}(\tau) \hat{a}_k^\dagger. \quad (13)$$

The orbitals $c_{\mu k}(\tau)$ obey orthonormality relations analogous to Eq. (4).

The equations of motion for imaginary time propagation can be derived analogously to the ones for real time propagation (an explicit derivation is given in the Appendix) and read

$$\begin{aligned} -\frac{dA_{i_1 \dots i_f}}{d\tau} &= \left\langle \Phi_{i_1 \dots i_f} \left| \hat{H} - \sum_{\nu, \mu=1}^f \hat{b}_\nu^\dagger \bar{h}_{\nu\mu} \hat{b}_\mu \right| \Psi \right\rangle, \quad (14) \\ -\frac{dc_{\mu k}}{d\tau} &= \sum_{\nu=1}^f \bar{h}_{\mu\nu} c_{\nu k} + \sum_{l=1}^F \left(\delta_{kl} - \sum_{\nu=1}^f c_{\nu k} c_{\nu l}^* \right) \\ &\quad \cdot \sum_{\lambda=1}^f \rho_{\mu\lambda}^{-1} \left\langle \Psi \left| \hat{b}_\lambda^\dagger [\hat{a}_l, \hat{H}]_{\hat{a}_i = \sum_{\kappa=1}^f c_{\kappa i} \hat{b}_\kappa} \right| \Psi \right\rangle. \end{aligned} \quad (15)$$

The only difference between real and imaginary time propagation is a change in the matrix resulting from the 'gauge' condition. The matrix

$$\bar{h}_{l\mu} = -\sum_{k=1}^F c_{lk}^* \frac{dc_{\mu k}}{d\tau}. \quad (16)$$

appearing in the imaginary time equations of motions is anti-hermitian. The evolution of the time-dependent

creation and annihilation operators is then given by

$$-\frac{d\hat{b}_\mu^\dagger}{d\tau} = -\sum_{k=1}^F \frac{dc_{\mu k}}{d\tau} \hat{a}_k^\dagger = -\sum_{k,l=1}^F c_{lk}^* \frac{dc_{\mu k}}{d\tau} \hat{b}_l^\dagger = \sum_{l=1}^F \bar{h}_{l\mu} \hat{b}_l^\dagger, \quad (17)$$

$$-\frac{d\hat{b}_\mu}{d\tau} = -\sum_{k=1}^F \frac{dc_{\mu k}^*}{d\tau} \hat{a}_k = -\sum_{k,l=1}^F c_{lk} \frac{dc_{\mu k}^*}{d\tau} \hat{b}_l = \sum_{l=1}^F \bar{h}_{l\mu}^* \hat{b}_l. \quad (18)$$

IV. 'GAUGE' CONDITIONS

The equations of motion Eq. (14) and (15) contain the 'gauge' matrix $\bar{h}_{\mu\nu}$ which introduces rotations in the space spanned by the orbitals $c_{\nu k}$. For a fixed number of basis functions the quality of the representation depends on the orbital rotations.¹⁰⁹ Thus, the choice of the 'gauge' matrix $\bar{h}_{\mu\nu}$ affects the accuracy of a MCTDH-oSQR calculation for a given basis size.

The typical choice for the 'gauge' matrix $\bar{h}_{\mu\nu}$ used in MCTDH calculations is

$$\bar{h}_{\mu\nu}^{(zero)} = 0. \quad (19)$$

This choice will be called *zero gauge* in the following. The zero gauge simplifies the equations of motions but does in general not minimize the correlation in the second quantization representation. In contrast, the use of a natural orbital representation minimizes the apparent correlation in a two particle system¹¹⁰ and approximately minimizes the correlation in a multi-particle system (see, e.g., Ref. 111 for a discussion of the issue). A natural orbital representation, which implies a diagonal form of the one-particle density matrix,

$$\rho_{\mu\nu}(\tau) = \delta_{\mu\nu} \rho_\nu(\tau), \quad (20)$$

can be retained during the propagation if a specific 'gauge' matrix $\bar{h}_{\mu\nu}^{(nat)}$ is employed. This choice is called *natural gauge* in the following.

The natural gauge matrix $\bar{h}_{\mu\nu}^{(nat)}$ can be derived by considering the time derivative of the one-particle density matrix:

$$\begin{aligned} \frac{d\rho_{\mu\nu}}{d\tau} &= \frac{d}{d\tau} \langle \Psi | \hat{b}_\mu^\dagger \hat{b}_\nu | \Psi \rangle \\ &= -\langle \Psi | \hat{H} \hat{b}_\mu^\dagger \hat{b}_\nu | \Psi \rangle - \langle \Psi | \hat{b}_\mu^\dagger \hat{b}_\nu \hat{H} | \Psi \rangle \\ &\quad + \left\langle \Psi \left| \frac{d\hat{b}_\mu^\dagger}{d\tau} \hat{b}_\nu \right| \Psi \right\rangle + \left\langle \Psi \left| \hat{b}_\mu^\dagger \frac{d\hat{b}_\nu}{d\tau} \right| \Psi \right\rangle \\ &= -\langle \Psi | \hat{H} \hat{b}_\mu^\dagger \hat{b}_\nu | \Psi \rangle - \langle \Psi | \hat{b}_\mu^\dagger \hat{b}_\nu \hat{H} | \Psi \rangle \\ &\quad - \sum_{\sigma=1}^f \bar{h}_{\sigma\mu} \rho_{\sigma\nu} - \sum_{\sigma=1}^f \bar{h}_{\sigma\nu}^* \rho_{\mu\sigma} \end{aligned} \quad (21)$$

Here the definition of the 'gauge' matrix from Eq. (16) was used. The derivative of the one particle density matrix can be written in compact form employing the anti-commutator $\{A, B\} = AB + BA$ and the anti-hermiticity of $\bar{h}_{\sigma\nu}$:

$$\frac{d\rho_{\mu\nu}}{d\tau} = -\langle \Psi | \left\{ \hat{H}, \hat{b}_\mu^\dagger \hat{b}_\nu \right\} | \Psi \rangle - \sum_{\sigma=1}^f (\bar{h}_{\sigma\mu} \rho_{\sigma\nu} - \bar{h}_{\nu\sigma} \rho_{\mu\sigma}). \quad (22)$$

In the natural orbital representation

$$0 = \frac{d\rho_{\mu\nu}}{d\tau} \quad (23)$$

and thus

$$\begin{aligned} 0 &= \langle \Psi | \left\{ \hat{H}, \hat{b}_\mu^\dagger \hat{b}_\nu \right\} | \Psi \rangle + \sum_{\sigma=1}^f (\bar{h}_{\sigma\mu}^{(nat)} \rho_{\sigma\nu} - \bar{h}_{\nu\sigma}^{(nat)} \rho_{\mu\sigma}) \\ &= \langle \Psi | \left\{ \hat{H}, \hat{b}_\mu^\dagger \hat{b}_\nu \right\} | \Psi \rangle + \bar{h}_{\nu\mu}^{(nat)} (\rho_\nu - \rho_\mu) \end{aligned} \quad (24)$$

has to be fulfilled for all $\mu \neq \nu$. Employing a regularization which guarantees that $\bar{h}_{\mu\nu} \rightarrow 0$ for $\rho_\mu - \rho_\nu \rightarrow 0$, one finally obtains

$$\bar{h}_{\nu\mu}^{(nat)} = \langle \Psi | \left\{ \hat{H}, \hat{b}_\mu^\dagger \hat{b}_\nu \right\} | \Psi \rangle \frac{\rho_\nu - \rho_\mu}{(\rho_\nu - \rho_\mu)^2 + \epsilon^2} \quad (25)$$

where ϵ is a small positive regularization constant.

It is interesting to compare the result for the imaginary time propagation, Eq. (25), with the one for the real-time propagation:

$$h_{\nu\mu}^{(nat)} = \langle \Psi | \left[\hat{H}, \hat{b}_\mu^\dagger \hat{b}_\nu \right] | \Psi \rangle \frac{\rho_\nu - \rho_\mu}{(\rho_\nu - \rho_\mu)^2 + \epsilon^2} \quad (26)$$

(see Ref. 109 for a derivation). At this point an important difference between the anti-commutator $\{\hat{H}, \hat{b}_\mu^\dagger \hat{b}_\nu\}$ in Eq. 25 and the commutator $[\hat{H}, \hat{b}_\mu^\dagger \hat{b}_\nu]$ in Eq. 26 should be noted. Considering Hamiltonians including up to N-particle operators, the commutator can include in maximum N-particle operators while the anti-commutator can include (N+1)-particle operators. This can be nicely illustrated for the one-particle Hamiltonian

$$\hat{H}^{(1)} = \sum_{\rho, \sigma=1}^f w_{\rho\sigma} \hat{b}_\rho^\dagger \hat{b}_\sigma. \quad (27)$$

Here one finds

$$\begin{aligned} \{\hat{H}, \hat{b}_\mu^\dagger \hat{b}_\nu\} &= \sum_{i,j=1}^f w_{\rho\sigma} \hat{b}_\rho^\dagger \hat{b}_\sigma \hat{b}_\mu^\dagger \hat{b}_\nu + \sum_{i,j=1}^f w_{\rho\sigma} \hat{b}_\rho^\dagger \hat{b}_\nu \hat{b}_i^\dagger \hat{b}_j \hat{b}_\sigma \\ &= 2 \sum_{\rho, \sigma=1}^f w_{i j} \hat{b}_\mu^\dagger \hat{b}_i^\dagger \hat{b}_j \hat{b}_\nu \\ &+ \sum_{\rho=1}^f w_{\rho\mu} \hat{b}_\rho^\dagger \hat{b}_\nu + \sum_{\sigma=1}^f w_{\nu\sigma} \hat{b}_\mu^\dagger \hat{b}_\sigma \end{aligned} \quad (28)$$

and

$$\begin{aligned} [\hat{H}, \hat{b}_\mu^\dagger \hat{b}_\nu] &= \sum_{i,j=1}^f w_{\rho\sigma} \hat{b}_\rho^\dagger \hat{b}_\sigma \hat{b}_\mu^\dagger \hat{b}_\nu - \sum_{i,j=1}^f w_{\rho\sigma} \hat{b}_\rho^\dagger \hat{b}_\nu \hat{b}_i^\dagger \hat{b}_j \hat{b}_\sigma \\ &= \sum_{\rho=1}^f w_{\rho\mu} \hat{b}_\rho^\dagger \hat{b}_\nu + \sum_{\sigma=1}^f w_{\nu\sigma} \hat{b}_\mu^\dagger \hat{b}_\sigma. \end{aligned} \quad (29)$$

This difference is of central importance for the numerical effort involved in the imaginary time propagation. If the system of interest is described by a N-Particle Hamiltonian and f orbitals, the effort to calculate $\langle \Psi | \left\{ \hat{H}, \hat{b}_\mu^\dagger \hat{b}_\nu \right\} | \Psi \rangle$ scales proportional to f^{2N+2} . In contrast, any other object present in the MCTDH-oSQR approach can be evaluated with an effort scaling as f^{2N} . Thus, the use of the natural gauge condition might reduce correlation but it significantly increases the numerical effort for a given number of orbitals.

Alternatively, a gauge reducing the spectral width of the effective operator driving the motion of the wave function can be considered. To this end, the measure

$$\Delta = \sum_{\mu} \left(\frac{d}{d\tau} \langle \hat{b}_\mu \Psi | \right) \left(\frac{d}{d\tau} | \hat{b}_\mu \Psi \rangle \right) \quad (30)$$

is minimized with respect to $h_{\mu\nu}$. The resulting 'gauge' will be called *spectral gauge* in the following. Employing $\frac{d\Psi}{d\tau} = -\hat{H}\Psi$ and Eqs. (17), (18), the measure Δ reads

$$\begin{aligned} \Delta &= \sum_{\mu=1}^f \langle \hat{b}_\mu \hat{H} \Psi | \hat{b}_\mu \hat{H} \Psi \rangle + \sum_{\mu, \nu=1}^f \langle \hat{b}_\mu \hat{H} \Psi | \bar{h}_{\nu\mu}^* \hat{b}_\nu \Psi \rangle \\ &+ \sum_{\mu, \nu=1}^f \langle \bar{h}_{\nu\mu}^* \hat{b}_\nu \Psi | \hat{b}_\mu \hat{H} \Psi \rangle + \sum_{\mu, \nu, \lambda=1}^f \langle \bar{h}_{\lambda\mu}^* \hat{b}_\lambda \Psi | \bar{h}_{\nu\mu}^* \hat{b}_\nu \Psi \rangle \\ &= \sum_{\mu=1}^f \langle \hat{b}_\mu \hat{H} \Psi | \hat{b}_\mu \hat{H} \Psi \rangle + \sum_{\mu, \nu=1}^f \bar{h}_{\nu\mu}^* \langle \hat{b}_\mu \hat{H} \Psi | \hat{b}_\nu \Psi \rangle \\ &+ \sum_{\mu, \nu=1}^f \bar{h}_{\nu\mu} \langle \hat{b}_\nu \Psi | \hat{b}_\mu \hat{H} \Psi \rangle + \sum_{\mu, \nu, \lambda=1}^f \bar{h}_{\lambda\mu} \bar{h}_{\nu\mu}^* \langle \hat{b}_\lambda \Psi | \hat{b}_\nu \Psi \rangle. \end{aligned} \quad (31)$$

If the anti-hermiticity of the \bar{h} -matrix is employed, one finds

$$\begin{aligned} \Delta &= \sum_{\mu=1}^f \langle \hat{b}_\mu \hat{H} \Psi | \hat{b}_\mu \hat{H} \Psi \rangle - \sum_{\mu, \nu=1}^f \bar{h}_{\mu\nu} \langle \hat{b}_\mu \hat{H} \Psi | \hat{b}_\nu \Psi \rangle \\ &+ \sum_{\mu, \nu=1}^f \bar{h}_{\nu\mu} \langle \hat{b}_\nu \Psi | \hat{b}_\mu \hat{H} \Psi \rangle - \sum_{\mu, \nu, \lambda=1}^f \bar{h}_{\lambda\mu} \bar{h}_{\mu\nu} \langle \hat{b}_\lambda \Psi | \hat{b}_\nu \Psi \rangle. \end{aligned} \quad (32)$$

Minimizing Δ with respect to $\bar{h}_{\sigma\xi}$ yields

$$\begin{aligned}
0 &= \frac{\partial\Delta}{\partial\bar{h}_{\sigma\xi}} \\
&= -\langle\Psi|\hat{H}\hat{b}_\sigma^\dagger\hat{b}_\xi|\Psi\rangle + \langle\Psi|\hat{b}_\sigma^\dagger\hat{b}_\xi\hat{H}|\Psi\rangle \\
&\quad - \sum_{\lambda=1}^f \bar{h}_{\lambda\sigma} \langle\hat{b}_\lambda\Psi|\hat{b}_\xi\Psi\rangle - \sum_{\nu=1}^f \bar{h}_{\xi\nu} \langle\hat{b}_\sigma\Psi|\hat{b}_\nu\Psi\rangle \\
&= -\langle\Psi|[\hat{H},\hat{b}_\sigma^\dagger\hat{b}_\xi]|\Psi\rangle - \sum_{\lambda=1}^f \bar{h}_{\lambda\sigma}\rho_{\lambda\xi} - \sum_{\lambda=1}^f \bar{h}_{\xi\lambda}\rho_{\sigma\lambda}.
\end{aligned} \tag{33}$$

Thus, the $\bar{h}^{(spec)}$ -matrix corresponding to the spectral gauge has to fulfill:

$$\sum_{\lambda=1}^f \left(\bar{h}_{\lambda\sigma}^{(spec)} \rho_{\lambda\xi} + \bar{h}_{\xi\lambda}^{(spec)} \rho_{\sigma\lambda} \right) = -\langle\Psi|[\hat{H},\hat{b}_\sigma^\dagger\hat{b}_\xi]|\Psi\rangle. \tag{34}$$

To obtain an explicit expression for $\bar{h}^{(spec)}$, one first transforms Eq. (34) into the natural orbital representation. The matrix u transforming from any given representation into the natural orbital representation can be obtained by diagonalizing the single-particle density matrix:

$$\tilde{\rho}_\mu = \sum_{\delta,\lambda=1}^f u_{\lambda\mu}^* \rho_{\lambda\delta} u_{\delta\mu}. \tag{35}$$

The transformed matrices and operators read

$$\tilde{h}_{\nu\mu} = \sum_{\delta,\lambda=1}^f u_{\lambda\mu}^* \bar{h}_{\delta\lambda} u_{\delta\nu}. \tag{36}$$

$$\hat{b}_\mu^\dagger = \sum_{\delta,\lambda=1}^f u_{\lambda\mu}^* \hat{b}_\lambda^\dagger \tag{37}$$

$$\hat{b}_\mu = \sum_{\delta,\lambda=1}^f u_{\lambda\mu} \hat{b}_\lambda \tag{38}$$

Eq. (34) then takes the simplified form

$$\tilde{h}_{\xi\sigma}^{(spec)} (\tilde{\rho}_\xi + \tilde{\rho}_\sigma) = \langle\Psi|[\hat{H},\hat{b}_\sigma^\dagger\hat{b}_\xi]|\Psi\rangle \tag{39}$$

Dividing by the regularized sum $\tilde{\rho}_\rho + \tilde{\rho}_\sigma + \epsilon$ yields an explicit expression for the spectral gauge matrix $\tilde{h}^{(spec)}$ in natural representation:

$$\tilde{h}_{\xi\sigma}^{(spec)} = \frac{\langle\Psi|[\hat{H},\hat{b}_\sigma^\dagger\hat{b}_\xi]|\Psi\rangle}{\tilde{\rho}_\xi + \tilde{\rho}_\sigma + \epsilon}. \tag{40}$$

Transformation to the original representation results in the working equation defining $\bar{h}_{\mu\nu}$ in the spectral gauge:

$$\bar{h}_{\mu\nu}^{(spec)} = \sum_{\xi,\sigma,\delta,\lambda=1}^f u_{\nu\sigma} \frac{u_{\lambda\sigma}^* \langle\Psi|[\hat{H},\hat{b}_\lambda^\dagger\hat{b}_\delta]|\Psi\rangle u_{\delta\xi}}{\tilde{\rho}_\xi + \tilde{\rho}_\sigma + \epsilon} u_{\mu\xi}^*. \tag{41}$$

Since this equation contains a commutator and not an anti-commutator, the numerical effort for the calculation of this so called spectral gauge scales proportional to f^{2N} if the solution of an N -Particle Hamiltonian is described by f orbitals. Moreover, the numerical results shown in Sec. VI indicate that the spectral gauge reduces the correlation in the wave function. A simple example that provides further insights into the advantages of the spectral gauge is discussed in Appendix B.

V. PARTICLE NUMBER CONSERVATION

In systems with particle number conserving Hamiltonians one is frequently interested in obtaining solutions with a fixed number of particles. The MCTDH-SQR and MCTDH-oSQR approaches employ the Fock space and thus contain states with all possible particle numbers. In principle, this does not constitute a problem for a numerically exact approach. In particle number conserving systems the particle number is a constant of motion and the particle number can be defined via the initial conditions chosen. However, in practical calculations numerical errors can result in small populations of states with incorrect particle numbers. This typically is not an important issue in real time propagations. Here small contributions to the wave function with incorrect particle numbers do not grow during the propagation for a particle number conserving Hamiltonians. In contrast, these numerical errors can cause serious problems in imaginary time propagation. Here small contributions to the wave function with incorrect particle numbers can grow exponentially during the propagation if these contributions show energies below the energies of relevant states with the correct particle number. In this situation, particle number conservation must be explicitly enforced to guarantee numerical stability.

Particle number conservation can be assured via a penalty term \hat{H}_{con} added to the system's Hamiltonian \hat{H}_{sys} . \hat{H}_{con} artificially increases the energy of states with particle numbers differing from the desired particle number N . Thus, the effective Hamiltonian

$$\hat{H} = \hat{H}_{sys} + \hat{H}_{con} \tag{42}$$

is used in the propagation. \hat{H}_{con} should not affect states showing the desired particle number N and strongly increase the energy of all states showing particle numbers deviating from N . A straightforward choice of \hat{H}_{con} would be

$$\hat{H}_{con} = \Gamma \cdot \left(\sum_{k=1}^F \hat{a}_k^\dagger \hat{a}_k - N \right)^2 \tag{43}$$

where Γ is a large positive number. Within the context of the present work, this operator has one significant disadvantage. In MCTDH-SQR and MCTDH-oSQR calculations the Hamiltonian is typically expanded in a sum

of products of single-particle operators. In the required form, \hat{H}_{con} reads

$$\hat{H}_{con} = \Gamma \cdot \sum_{k=1}^F \sum_{l=1}^F \hat{a}_k^\dagger \hat{a}_k \hat{a}_l^\dagger \hat{a}_l - 2\Gamma \cdot N \cdot \sum_{k=1}^F \hat{a}_k^\dagger \hat{a}_k + N^2. \quad (44)$$

Thus, the addition of \hat{H}_{con} gives rise to $F^2 + F + 1$ additional terms in the Hamiltonian.

A more efficient choice of \hat{H}_{con} is¹¹²

$$\hat{H}_{con} = \frac{2\Gamma}{\zeta^2} \cdot \cosh \left(\zeta \left(\sum_{k=1}^F \hat{a}_k^\dagger \hat{a}_k - N \right) \right) - \frac{2\Gamma}{\zeta^2} \quad (45)$$

where Γ is a large positive number and ζ is a small positive number. A Taylor expansion of this operator in ζ ,

$$\hat{H}_{con} \approx \Gamma \cdot \left(\sum_{k=1}^F \hat{a}_k^\dagger \hat{a}_k - N \right)^2 + \frac{\zeta^2 \Gamma}{12} \cdot \left(\sum_{k=1}^F \hat{a}_k^\dagger \hat{a}_k - N \right)^4, \quad (46)$$

demonstrates that this operator and the \hat{H}_{con} of Eq. (43) are asymptotically equivalent for small ζ . Rewriting Eq. (45) in sum of products form results in

$$\hat{H}_{con} = \frac{2\Gamma}{\zeta^2} \left(e^{\zeta N} \prod_{k=1}^F e^{\zeta \hat{a}_k^\dagger \hat{a}_k} + e^{-\zeta N} \prod_{k=1}^F e^{-\zeta \hat{a}_k^\dagger \hat{a}_k} \right) - \frac{2\Gamma}{\zeta^2}. \quad (47)$$

This operator gives rise to only three additional terms in the Hamiltonian. Since a non-trivial \hat{H}_{sys} consists of more than F terms, the additional effort resulting from the application of this \hat{H}_{con} is small compared to numerical effort required for the application of \hat{H}_{sys} .

VI. NUMERICAL EXAMPLES

A. Implementation and Numerical Details

Quantum dynamics calculations studying different Bose Hubbard models are used to illustrate different aspects of the methodology discussed above. ML-MCTDH-SQR and ML-MCTDH-oSQR propagation in imaginary time propagation is employed to calculate the respective ground states. A constant mean field (CMF) approach^{113,114} is used to integrate the ML-MCTDH-SQR and ML-MCTDH-oSQR equations of motion.

In the ML-MCTDH-SQR calculations the CMF2 scheme of Ref. 114 is employed. Since results obtained with different integration accuracies will be compared in the context of the particle number conservation, a detailed description of the different relevant parameters will be given in the following. The CMF approach employs

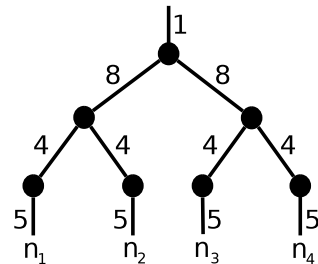


Figure 1. Diagrammatic representation of ML-MCTDH-SQR wave function used in Sect. VIA. See Refs. 4 and 109 for a detailed description of the diagrammatic notation. The occupation number n_i of the i -th site takes the role of the i -th coordinate in the MCTDH-SQR approach.

a two level integration scheme with different time steps used to update matrix elements and to integrate the equations of motion for the expansion coefficients and the single-particle functions. Here a common accuracy parameter ϵ is used to control the time steps at all levels: an accuracy parameter of $10 \cdot \epsilon$ is used in the CMF update step (see Eq.(27) of Ref. 114 for the definition of the error estimate) and an accuracy parameter ϵ is employed in the Bulirsch-Stoer integrator used to integrate the individual equations of motion (see Ref. 115 for the definition of the error measure). Furthermore, the same ϵ is used regularization constant in the computation of the inverse density matrices.

In the ML-MCTDH-oSQR approach the optimized orbitals $c_{\mu,k}(t)$ have to be propagated in addition to the expansion coefficients and single-particle functions of the ML-MCTDH ansatz already presented in the ML-MCTDH-SQR approach. Here an extended version of the CMF2 scheme is used which treats the MCTDH-oSQR orbitals analogously to the single-particle functions (SPFs) in the ML-MCTDH approach. The 'gauge' matrix $\tilde{h}_{\mu\nu}$, the one particle density matrix

$$\langle \Psi | \hat{b}_\sigma^\dagger \hat{b}_\xi | \Psi \rangle, \quad (48)$$

and the two particle density matrix

$$\langle \Psi | \hat{b}_\lambda^\dagger \hat{b}_\nu^\dagger \hat{b}_\kappa \hat{b}_\mu | \Psi \rangle \quad (49)$$

are only computed at CMF update steps. All other objects appearing in the equations of motion of the optimized orbitals $c_{\mu,k}(t)$ can be written as functions of the one and two particle density matrices and the time-dependent orbitals $c_{\mu,k}(t)$. The integration of the orbital equations of motion in the CMF approach then considers the full time-dependence of the orbitals explicitly but assumes the gauge, one particle density, and two particle density matrix elements do not change during a CMF integration period. A Bulirsch-Stoer scheme is employed for this integration. The common regularization parameter ϵ is used in the implementation of Eqs. (15), (25) and (41).

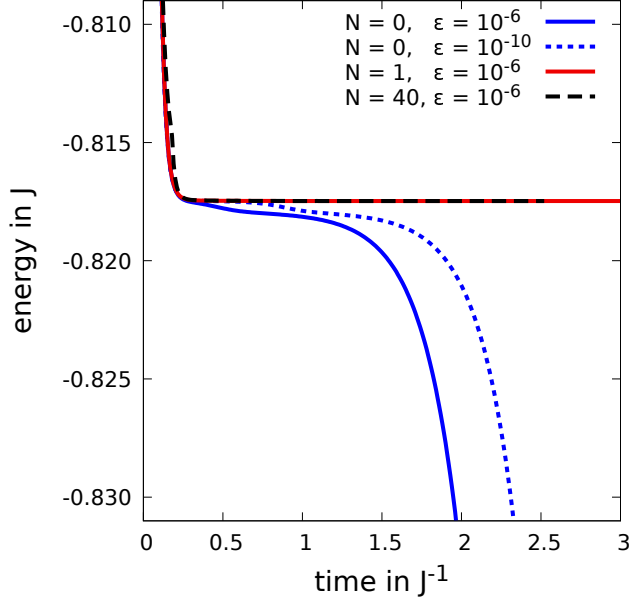


Figure 2. The energy is displayed as a function of the (imaginary) propagation time for different ML-MCTDH-SQR calculations. Results obtained with ($\Gamma = 1, \Gamma = 40$) and without ($\Gamma = 0$) a constraint operator ensuring particle number conservation are displayed. Red and dashed black lines display results computed with constraint operators with $\Gamma = 1$ and $\Gamma = 40$, respectively. Solid and dotted blue lines show results of unconstrained calculations obtained with different integration accuracies ($\epsilon = 10^{-6}$ and $\epsilon = 10^{-10}$, respectively).

B. Particle Number Conservation

First, the particle number conservation in the ML-MCTDH-SQR approach and the effect of the constraint operator \hat{H}_{con} given in Eq.(45) is studied. Here a Bose Hubbard model described by the Hamiltonian

$$\hat{H}_{Sys} = -J \sum_{i=1}^F (\hat{a}_i^\dagger \hat{a}_{i+1} + \hat{a}_{i+1}^\dagger \hat{a}_i) + \frac{1}{2} U \sum_{i=1}^F (\hat{a}_i^\dagger)^2 \hat{a}_i^2 \quad (50)$$

is used. Twenty sites, $F = 20$ and four particles, $N = 4$, are considered and the unity values of the parameters J and U are assumed, $J = U = 1$. Starting from the initial state

$$|\Psi(0)\rangle = \hat{a}_1^\dagger \hat{a}_2^\dagger \hat{a}_3^\dagger \hat{a}_4^\dagger |0\rangle, \quad (51)$$

the ground state is computed by imaginary time propagation. The ML-MCTDH-SQR wave function representation is given in Fig. (1) (see Refs. 4 and 109 for a detailed description of the diagrammatic notation). This representation assures convergence with respect to the number of single-particle functions employed.

In Fig. 2, the energy relaxation during the imaginary time propagation obtained from different calculations is

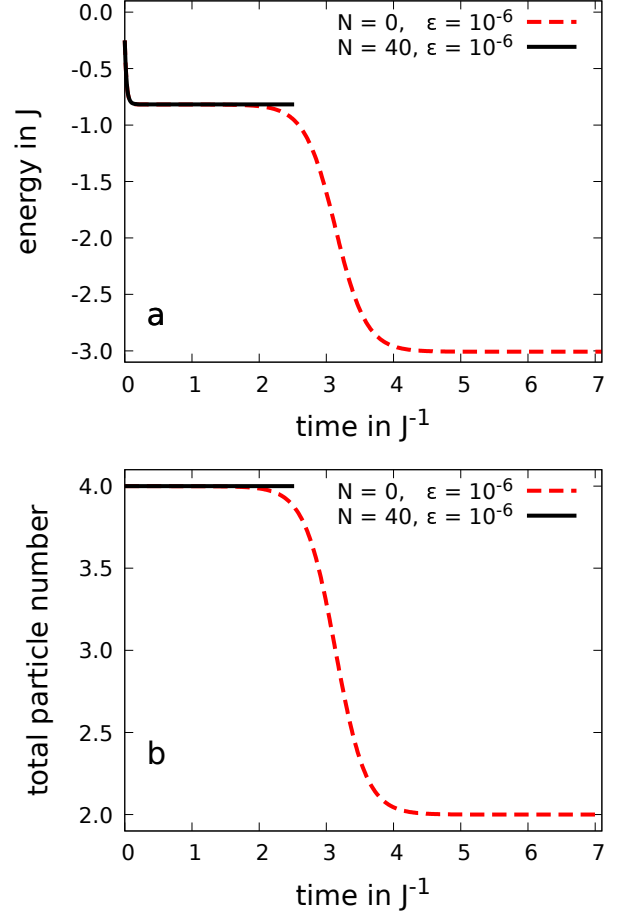


Figure 3. The expectation values of energy and particle number are displayed as functions of imaginary time in panels (a) and (b), respectively. The black lines display the result of a calculation employing a constraint operator ensuring particle number conservation ($\Gamma = 40$). The dashed red line shows the result obtained without constraint operator ($\Gamma = 0$).

shown. Results obtained by straightforward calculations without constraint operator are given by blue lines. Results computed using the constraint operator specified in Eq.(45) with parameter values $\zeta = 1/16$, $\Gamma = 1$ or $\zeta = 1/16$, $\Gamma = 40$ are displayed by red or dashed black lines, respectively. One immediately finds that the constrained calculations quickly converge to a ground state energy $E_0 = 0.817 J$. This result is independent of the specific choice of the parameter Γ . In the unconstrained calculations, the energy initially decays towards E_0 , then stabilizes at values close to E_0 for an intermediate time period, and finally decays towards unphysically low values.

Furthermore, the results of the constrained calculations crucially depend on the integration accuracy: the solid blue line in Fig. 2 shows the result obtained with the standard integration accuracy $\epsilon = 10^{-6}$ while the result of a high accuracy integration with $\epsilon = 10^{-10}$ is displayed

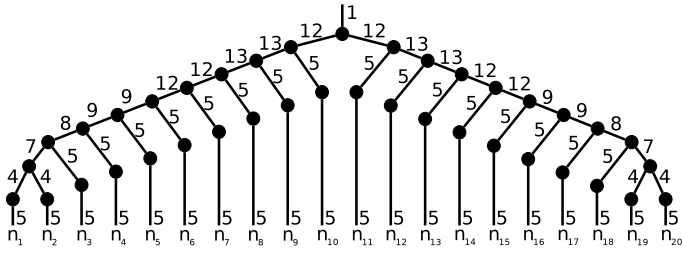


Figure 4. Graphical representation of the wavefunction used in the converged ML-MCTDH-SQR wavefunction reference calculations discussed in Sect. VI C.

as dotted blue line. The more accurate calculation clearly shows a more extended intermediate plateau at energies close to E_0 . This finding confirms the expectation that a perfectly accurate integration should converge to the correct values even without the use a constraint operator.

The connection between particle number conservation and numerical stability is demonstrated in Fig. 3. Comparing results obtained with and without use of the constraint operator (displayed by black solid and red dashed lines, respectively), panel (a) displays the expectation value of energy and panel (b) shows the expectation values of the particle number as a function of the (imaginary) propagation time. One clearly sees that the unphysical decay of the expectation value of energy coincides with the breakdown of the particle number conservation. The unconstrained calculation finally converges towards a final state which shows a particle number of two and an energy of $-3J$. The presence of a two-particle state with a lower energy in the Fock space thus causes the instability of the unconstrained ML-MCTDH-SQR calculation.

C. MCTDH-oSQR in Imaginary Time

The second numerical example studies single-layer and multi-layer MCTDH-oSQR propagation in imaginary time for a particle number conserving Hamiltonian. Here a Bose-Hubbard model with $N = 4$ bosons on $F = 20$ sides described by the Hamiltonian

$$\begin{aligned} \hat{H} = & -J \sum_{i=1}^F \left(\hat{a}_i^\dagger \hat{a}_{i+1} + \hat{a}_{i+1}^\dagger \hat{a}_i \right) + \frac{1}{2} U \sum_{i=1}^F \left(\hat{a}_i^\dagger \right)^2 \hat{a}_i^2 \\ & + \sum_{i=1}^F \frac{1}{2} \omega^2 \left(i - \frac{F+1}{2} \right)^2 \hat{a}_i^\dagger \hat{a}_{i+1}. \end{aligned} \quad (52)$$

with the parameter values $J = 1$, $U = 1$, $\omega = 0.1$ is studied. This model has previously been used to illustrate the MCTDHB approach¹¹⁶ is employed. Particle number conservation is explicitly enforced by the penalty operator \hat{H}_{con} given in Eq. (45) with $\Gamma = 500$ and $\zeta = 0.05$.

A converged reference solution was calculated using the ML-MCTDH-SQR approach. The diagrammatic representation of the wave function employed is given in Fig. 4.

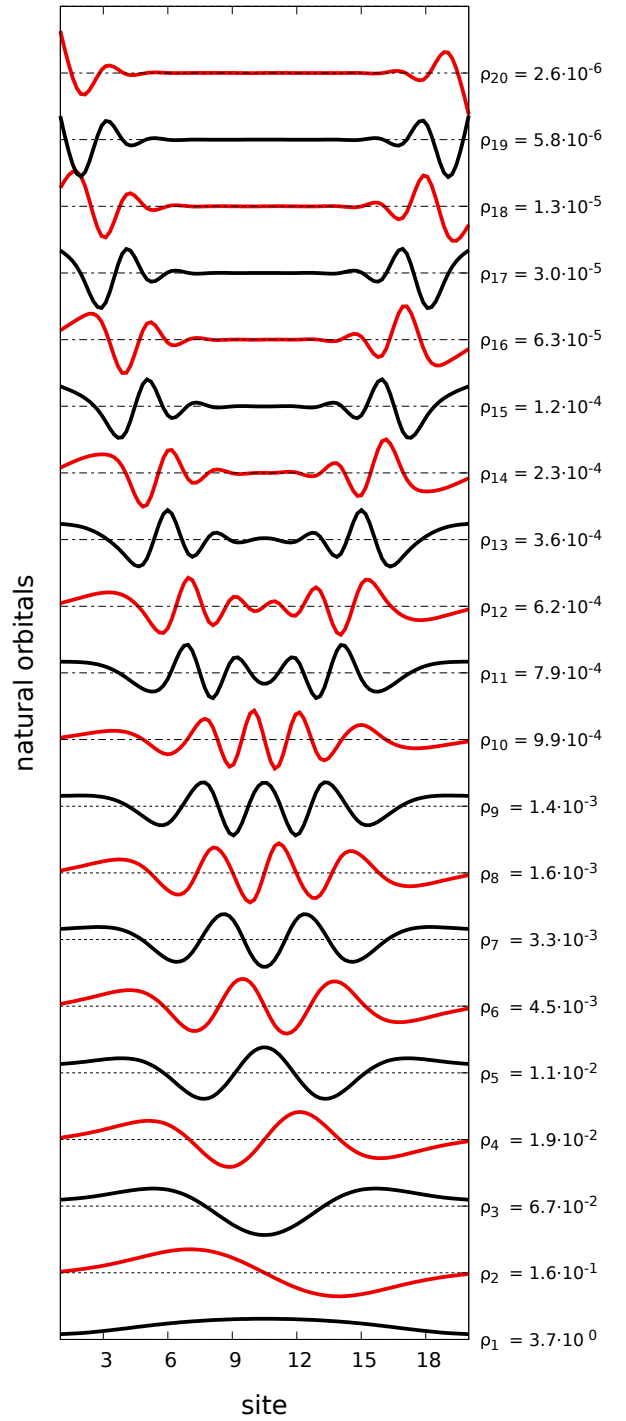


Figure 5. Natural orbitals obtained from the reference calculation described in Sec. VI C: the amplitude $c_{\mu k}$ of the natural orbital μ is displayed as a function of the side index k . The occupation number n_μ of each natural orbital μ is given.

A ground state energy of $E_{orb=20}^{FCI} = -7.3602(4)J$ is obtained. Natural orbitals are computed by diagonaliz-

ing the one particle density matrix

$$\rho_{ij} = \langle \Psi | \hat{a}_i^\dagger \hat{a}_j | \Psi \rangle \quad (53)$$

for the ground state Ψ . In Fig. 5, the amplitudes $c_{\mu k}$ of the natural orbitals are plotted and the natural populations ρ_μ are given. A dominant fraction of the total population is found in a single natural orbital: the population of the first natural orbital, $\rho_1 = 3.7$, accounts for 93% of the total particle number of 4. The population of the second most populated natural orbital is more than a factor of 20 smaller. The populations of the further natural orbitals then decrease roughly exponentially. However, the decay is rather slow following roughly a $\rho_{\mu-1}/\rho_\mu \approx 2$ rule. Based on these results, one can expect that a configuration interaction (CI) expansion in optimized orbitals yields reasonably accurate results with small numbers of orbitals but requires large number of orbitals to achieve high accuracies. These expectations will be confirmed by the results of the MCTDH-oSQR calculations presented in the following.

The investigation of the imaginary time propagation in the MCTDH-oSQR approach will first address the issue of the ‘gauge’ dependence discussed in Sect.IV. To this end, MCTDH-oSQR calculations employing the zero gauge, the natural gauge, and the spectral gauge are compared. The calculations employ 4 optimized orbitals. The initial state at the start of the imaginary time propagation, $\Psi(0)$, shows all 4 particles in a single orbital, i.e.,

$$|\Psi\rangle = \frac{1}{\sqrt{4!}} (\hat{b}_1^\dagger)^4 |0\rangle. \quad (54)$$

The initial occupied orbital is the symmetric linear combination of all F sides, $c_{1k} = 1/\sqrt{F}$, $k = 1, \dots, F$. The real Bloch states

$$c_{2k} = \frac{1}{\sqrt{2F}} \sin(2\pi(k-0.5)/F), \quad (55)$$

$$c_{3k} = \frac{1}{\sqrt{2F}} \cos(2\pi(k-0.5)/F), \quad (56)$$

$$c_{4k} = \frac{1}{\sqrt{2F}} \sin(4\pi(k-0.5)/F) \quad (57)$$

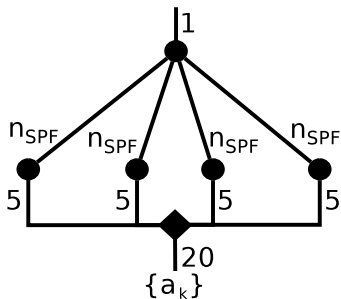


Figure 6. Diagrammatic representation of MCTDH-oSQR wavefunction discussed in Sect.VIC.

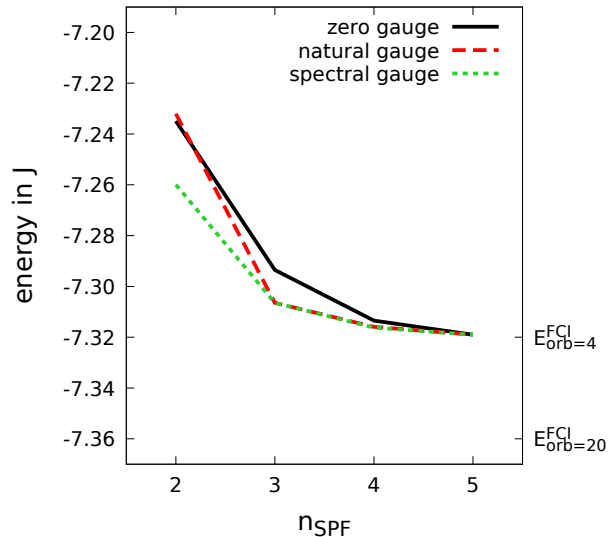


Figure 7. Comparison of MCTDH-oSQR results obtained with zero gauge (solid black line), natural gauge (dashed red line), and spectral gauge (dotted green line), using the wavefunction representation depicted in Fig. 6. The computed ground state energies are displayed as a function of the number of SPFs, n_{SPF} . The energy $E_{orb=20}^{FCI}$ computed by an exact ML-MCTDH-SQR calculations, and the energy $E_{orb=4}^{FCI}$, the MCTDH-oSQR result with four active orbitals converged with respect to the number of SPFs, are indicated.

are chosen as the three initially unoccupied orbitals in the MCTDH-oSQR calculation. The unoccupied SPFs are determined by the scheme described in Refs. 117 and 118.

Results of calculations employing the MCTDH-oSQR representation diagrammatically depicted in Fig. 6 with different numbers of SPFs n_{SPF} are shown in Fig. 7. The computed ground state energy is displayed as a function of n_{SPF} for calculations employing the zero gauge, the natural gauge, and the spectral gauge. One finds that the optimal results for the ground state energy which can be obtained with 4 active orbitals is $E_{orb=4}^{FCI} = -7.32 J$. This energy is $0.04 J$ larger than the accurate ground state energy $E_{orb=20}^{FCI} = -7.36 J$ obtained by the reference calculations. Comparing the results obtained with different ‘gauges’, differences in the convergence with respect to the number of SPFs can be seen in Fig. 7. Calculations employing the zero gauge converge more slowly than calculations employing the natural gauge or the spectral gauge. Results obtained with the natural gauge and the spectral gauge are essentially identical for $n_{SPF} > 2$. Surprisingly, for $n_{SPF} = 2$ the spectral gauge provides significantly better results than the natural gauge. This result is presumably an artifact of the natural gauge calculation resulting from incomplete convergence in the imaginary time propagation (see below for a more detailed discussion). Considering the difference in the numerical effort

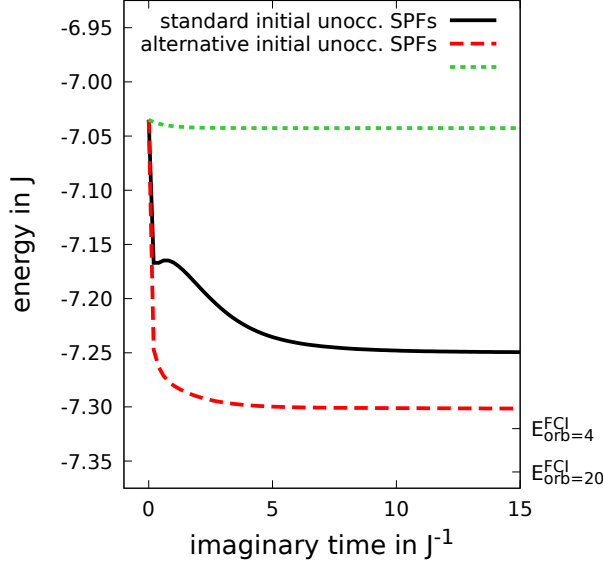


Figure 8. The dependence of the MCTDH-oSQR results with $n_{SPF} = 2$ and four active orbitals (see Fig. 6 for the diagrammatic representation of the wavefunction) on the choice of the initially unoccupied SPFs is shown. The energy is displayed as a function of imaginary time for initial unoccupied single particle functions calculated by the scheme of Ref.117 and 118 (solid black line) and for the two alternative choices (dash red and dotted green lines) described in the text. The energies $E_{orb=20}^{FCI}$ and $E_{orb=4}^{FCI}$ are indicated.

for the different gauges discussed in Sect.IV, these results strongly suggest that the spectral gauge is the most favorable choice.

As already noted above, we found that the MCTDH-oSQR propagation in imaginary time sometimes does not converge towards the optimal result for the given number of SPFs. An inspection of the wavefunctions appearing in the calculations reveals an important property: all single-particle functions show distinct local particle numbers which are preserved during the entire imaginary time propagation.

In a single-layer MCTDH-oSQR, the local particle number of the SPF $\phi_i^{(\kappa)}$ is defined via the occupation operator

$$\hat{n}^\kappa = \hat{b}_\kappa^\dagger \hat{b}_\kappa. \quad (58)$$

If two degrees of freedom ν and μ are combined into a group λ in the ML-MCTDH-oSQR approach, the local particle number for the group can analogously be defined via the occupation operator

$$\hat{n}^\lambda = \hat{n}^\nu + \hat{n}^\mu. \quad (59)$$

The generalization of this concept to an arbitrary tree structure is straightforward (note that in the following the standard notation introduced in Ref. 4 will be used to specify objects appearing in the multi-layer approach).

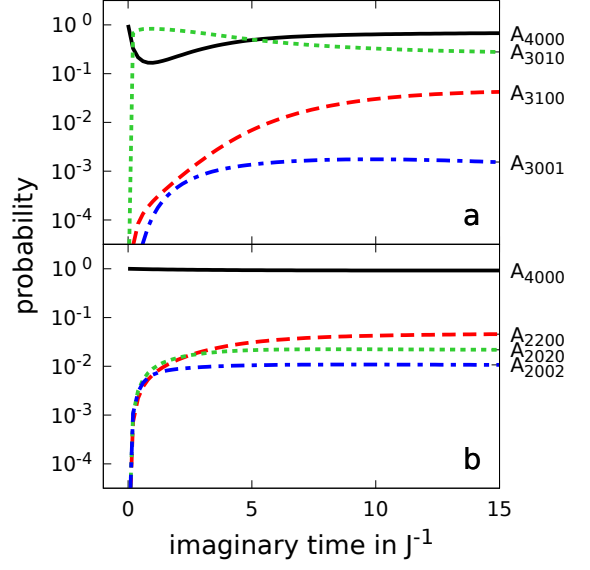


Figure 9. Non vanishing coefficients $A_{i_1 \dots i_4}$ in the MCTDH-oSQR imaginary time propagation with $n_{SPF} = 2$ and four active orbitals (see Fig. 6 for the diagrammatic representation of the wavefunction). The choice of the initially unoccupied SPFs differs in panel (a) and (b): in panel (a) the scheme of Ref.117 and 118 is employed while in panel (b) the alternative choice corresponding to the red dashed line in Fig.8 is used. See text for further details.

Thus, the statement that a SPF ϕ_i^λ shows a distinct local particle number n_i^κ implies

$$\hat{n}^\lambda \phi_i^\lambda = n_i^\lambda \phi_i^\lambda. \quad (60)$$

The local particle number conservation can be related to the convergence problems mentioned above. To this end, the ground state of the Bose-Hubbard model was calculated employing four orbitals and two SPFs per orbital (corresponding to $N = 2$ in Fig. 6). The spectral gauge and the same initial orbitals as in the above calculations have been employed. Orbital 1 is initially populated by four bosons ($n^1 = 4$) while orbitals 2 to 4 are unoccupied ($n^2 = n^3 = n^4 = 0$). The procedure of Refs. 117 and 118 used above then yields an unoccupied SPF with the local particle number $n^1 = 3$ associated with the orbital 1 and unoccupied SPFs with local particle numbers $n^\lambda = 1$ associated with the unoccupied orbitals $\lambda = 2, 3, 4$. The result for this choice of initial SPFs has been depicted Fig. 7. For comparison, two alternative sets of choices for the initial unoccupied SPFs have been considered. Here the local particle number of the unoccupied SPF associated with the orbital 1 is $n^1 = k$ with $k = 1$ or $k = 2$. The corresponding choices for local particle number of the unoccupied SPFs associated with the unoccupied orbitals $\lambda = 2, 3, 4$ are $n^\lambda = 4 - k$.

The result of imaginary time propagations starting from the three different initial choices of the unoccupied SPFs are shown in Fig. (8). In the figure, the energy

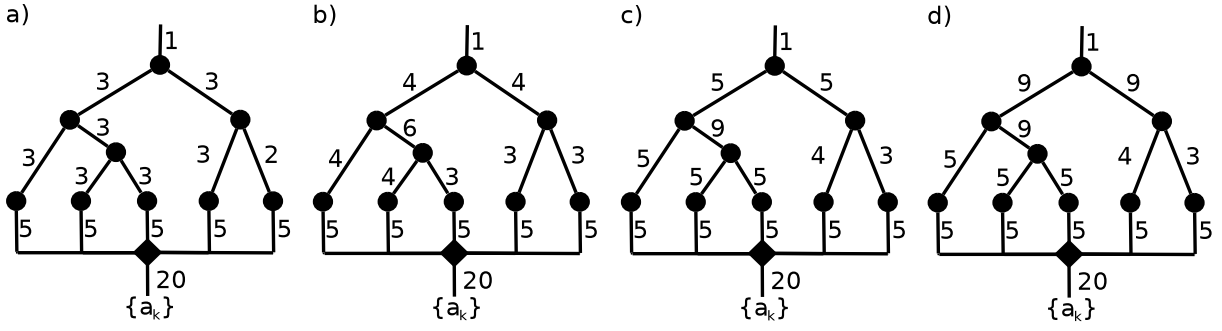


Figure 10. Diagrammatic representations of the different wavefunctions employed in the ML-MCTDH-oSQR calculations are shown in panels (a) to (d).

is displayed as a function of the imaginary time and the $E_{orb=4}^{FCI}$ and $E_{orb=20}^{FCI}$ values obtained from previous calculations are indicated. Most strikingly, a strong dependence of the computed energy on the initial choice of the unoccupied SPFs is observed. The alternative choice $k = 1$ (dotted green line) yields an energy curve which shows almost no decay while the alternative choice $k = 2$ yields strongly decaying energies converging to a final value close to $E_{orb=4}^{FCI}$, the $n_{SPF} \rightarrow \infty$ limit for four active orbitals found in Fig. 7. Remarkably, results obtained with the alternative choice $k = 2$ for the unoccupied SPFs converges to a lower energy than the result obtained with the “optimal” choice for the unoccupied SPFs according to Refs. 117 and 118.

Further insights can be gained by a detailed analysis of the MCTDH-oSQR wavefunctions obtained by the standard and the alternative ($k = 2$) choice of the unoccupied initial SPFs. In both cases the MCTDH-oSQR wavefunction (as defined in Eqs. (11)-(13) shows only four non-vanishing A-coefficients in the CI expansion (Eq. (12)): the wavefunction takes the form

$$\begin{aligned}
 |\Psi(\tau)\rangle &= A_{4000}(\tau) |\Phi_{4000}(\tau)\rangle + A_{3100}(\tau) |\Phi_{3100}(\tau)\rangle \\
 &+ A_{3010}(\tau) |\Phi_{3010}(\tau)\rangle + A_{3001}(\tau) |\Phi_{3001}(\tau)\rangle
 \end{aligned}
 \quad (61)$$

for the standard choice of the unoccupied initial SPFs and

$$\begin{aligned}
 |\Psi(\tau)\rangle &= A_{4000}(\tau) |\Phi_{4000}(\tau)\rangle + A_{2200}(\tau) |\Phi_{2200}(\tau)\rangle \\
 &+ A_{2020}(\tau) |\Phi_{2020}(\tau)\rangle + A_{2002}(\tau) |\Phi_{2002}(\tau)\rangle
 \end{aligned}
 \quad (62)$$

for the alternative choice of the unoccupied initial SPFs. The observed structures in the wavefunctions are a consequence of the local particle number conservation and the respective choice of the initial SPFs. The squared absolute values of the non-vanishing A_{ijkl} , i.e., the probabilities to occupied a configuration with the local particle numbers i, j, k, l in the four orbitals, are shown in Fig. 9 as a function of the imaginary time τ .

The results shown in Fig. 9 provide the insights which allow one to understand to data displayed in Figs. (8).

The “optimal” choice for the unoccupied SPFs introduced in Ref.117 is actually based a time-local definition of “optimal” referring to the initial time $\tau = 0$. Populating a second configuration with the local particle numbers 3, 0, 1, 0 yields a strong initial decrease of the energy in accordance with the time-local measure of the “optimal” choice of unoccupied SPFs used in Refs.117. While this choice provides favorable results for short propagation times τ , it does not allow for convergence to the optimal result for $\tau \rightarrow \infty$. In contrast, the wavefunction structure resulting from the alternative choice of the initial SPFs, Eq.(62), facilitates convergence towards lower final energies once the orbitals have been adapted. While the interplay between SPF and orbital optimization allows for a smooth exponential energy decay for the alternative choice, a more complex relaxation behavior is found for the standard choice in Figs. 8 and 9.

Based on the detailed understanding of the MCTDH-oSQR approach obtained above, its multi-layer extension will be studied in the following. The same Hamiltonian and initial wavefunction as in the previous MCTDH-oSQR calculations is used. Five orbitals and the wave function representations diagrammatically depicted in Fig. 10 are employed. The unoccupied initial SPFs have been individually chosen based on results of test calculations to assure optimal results. A two step procedure is employed to efficiently compute the ground state energy. First, the SPFs are propagated in imaginary time using frozen orbitals. Then the SPFs and orbitals are simultaneously propagated in imaginary time until convergence.

To investigate the convergence of the ML-MCTDH-oSQR approach with respect to the number of SPFs for a fixed number of orbitals, different SPF basis set sizes have been considered according to different upper limits ρ_{limit} for the population of the least populated natural SPF present in the wavefunction representation. The SPF bases given in panels (a), (b), (c), (d) of Fig. 10 guarantee that the smallest natural population is below $2.5 \cdot 10^{-3}$, $1 \cdot 10^{-3}$, $1 \cdot 10^{-4}$, $1 \cdot 10^{-5}$, respectively. The ground state energies obtained in the calculations are plotted in Fig.11 as a function of the ρ_{limit} value employed. The energy $E_{orb=5}^{FCI}$ computed with a extremely well converged SPF basis and five active orbitals as well as the previously

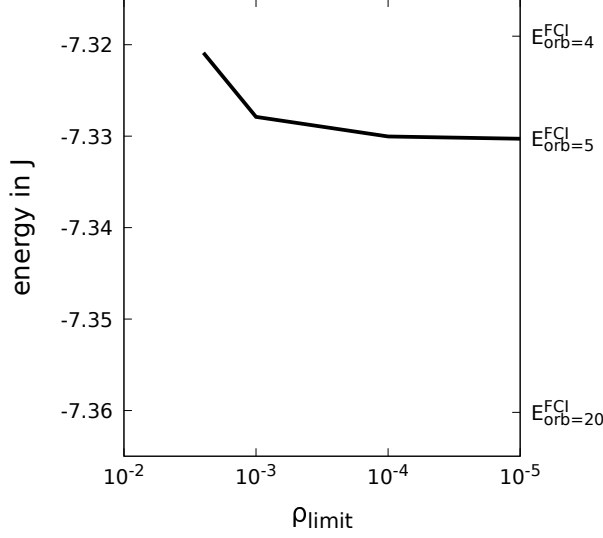


Figure 11. Convergence of the ML-MCTDH-oSQR calculation with respect to the number of SPFs: the computed ground state energy is displayed as a function of ρ_{limit} (see text for details). The diagrammatic representation of the different wavefunctions is given by Fig. (10). The energies $E_{orb=20}^{FCI}$ and $E_{orb=4}^{FCI}$ are indicated.

calculated energies $E_{orb=4}^{FCI}$ and $E_{orb=20}^{FCI}$ are indicated in the figure.

Roughly exponential convergence of the calculated energies towards $E_{orb=5}^{FCI}$ as a function of ρ_{limit} is found in Fig.11. The smallest basis considered, which corresponds to $\rho_{limit} = 2.5 \cdot 10^{-3}$, already yields an energy below $E_{orb=4}^{FCI}$, the best result obtainable with 4 active orbitals and almost converged results can be obtained with the basis corresponding to $\rho_{limit} = 1 \cdot 10^{-3}$. It is interesting to compare the effects resulting from the limited size of SPF bases and the limited number of active orbitals considered. As indicated in Fig.5, the population of the fifth natural orbital is $1.1 \cdot 10^{-2}$. The present results show that restricting the number of active orbitals to four and neglecting the fifth orbital results in a slightly larger error than using SPF basis sets corresponding to $\rho_{limit} = 2.5 \cdot 10^{-3}$. Thus, the respective populations of the natural orbitals and SPFs can be used to roughly estimate the relative importance of errors resulting from the limited numbers of orbitals and SPFs considered.

VII. DISCUSSION

A central result of the preceding section is the observation of a local particle number conservation in the individual SPFs employed in the single-layer and multi-layer MCTDH wavefunctions. This local particle number conservation has severe consequences. On one hand, it constrains the space available for the wavefunction during

the imaginary time propagation depending on the initial choice of the individual SPFs. This feature severely complicates the convergence behavior. On the other hand, the local particle number conservation results in large numbers of vanishing A -coefficients and could be employed to reduce the numerical effort. In this section, we first provide an analytical derivation of the local particle number conservation observed in the numerical study. Second, a revised ML-MCTDH-oSQR scheme which explicitly considers local particle number conservation in the multi-layer wavefunction representation will be suggested.

A. Local Particle Number Conservation

The local particle number conservation of the single particle functions in (multi-layer) MCTDH-SQR type approaches observed in the numerical study can be derived analytically. To this end, a particle number conserving Hamiltonian

$$[\hat{H}, \hat{N}] = 0, \quad (63)$$

where \hat{N} denotes the particle number operator,

$$\hat{N} = \sum_{k=1}^F \hat{a}_k^\dagger \hat{a}_k = \sum_{\mu=1}^F \hat{a}_\mu^\dagger \hat{a}_\mu, \quad (64)$$

and a wavefunction $|\Psi\rangle$ containing N particles,

$$\hat{N}\Psi = N\Psi, \quad (65)$$

is considered. The local particle number operator \hat{n}^λ associated with an arbitrary SPF ϕ_i^λ in the multi-layer MCTDH representation has been defined via Eqs. 58 and 59). Single-hole functions Ψ_i^λ corresponding to the SPFs ϕ_i^λ can be defined via

$$\Psi = \sum_i \Psi_i^\lambda \phi_i^\lambda \quad (66)$$

and the complementary operator \hat{N}^λ associated with the single-hole function Ψ_i^λ is given by

$$\hat{N}^\lambda = \hat{N} - \hat{n}^\lambda. \quad (67)$$

Using the above definitions, one can obtain equations describing the action of \hat{N}^λ on the single hole functions and \hat{n}^λ on the SPFs:

$$\begin{aligned} \hat{N}^\lambda |\Psi_j^\lambda\rangle &= \hat{N}^\lambda \langle \phi_j^\lambda | \Psi \rangle \\ &= \langle \phi_j^\lambda | \hat{N}^\lambda | \Psi \rangle \\ &= \langle \phi_j^\lambda | \hat{N} - \hat{n}^\lambda | \Psi \rangle \\ &= \sum_m \langle \phi_j^\lambda | N - \hat{n}^\lambda | \phi_m^\lambda \rangle |\Psi_m^\lambda\rangle \\ &= N |\Psi_m^\lambda\rangle - \sum_m \langle \phi_j^\lambda | \hat{n}^\lambda | \phi_m^\lambda \rangle |\Psi_m^\lambda\rangle \end{aligned} \quad (68)$$

and

$$\begin{aligned}
\hat{n}^\lambda \phi_j^\lambda &= \hat{n}^\lambda \langle \Psi_j^\lambda | \Psi \rangle \\
&= \langle \Psi_j^\lambda | \hat{n}^\lambda | \Psi \rangle \\
&= \langle \Psi_j^\lambda | (\hat{N} - \hat{N}^\lambda) | \Psi \rangle \\
&= \langle \Psi_j^\lambda | (N - \hat{N}^\lambda) | \Psi \rangle \\
&= N \phi_j^\lambda - \sum_m \phi_m^\lambda \langle \Psi_j^\lambda | \hat{N}^\lambda | \Psi_m^\lambda \rangle. \quad (69)
\end{aligned}$$

Thus, $\hat{n}^\lambda \phi_j^\lambda$ is located in the space spanned by the SPFs ϕ_m^λ and consequently

$$0 = (1 - \hat{P}^\lambda) \hat{n}^\lambda \phi_j^\lambda \quad (70)$$

where

$$\hat{P}^\lambda = \sum_m |\phi_m^\lambda\rangle \langle \phi_m^\lambda| \quad (71)$$

projects on the space spanned by the SPFs ϕ_m^λ .

In the next step the time-derivative of the matrix element

$$n_{jm}^\lambda = \langle \phi_j^\lambda | \hat{n}^\lambda | \phi_m^\lambda \rangle \quad (72)$$

is considered. In the MCTDH approach in second quantization representation the local particle number operator take the role of coordinate operators and can be considered as time-independent. Thus,

$$\frac{dn_{jm}^\lambda}{dt} = \left\langle \frac{\partial \phi_j^\lambda}{\partial t} \left| \hat{n}^\lambda \right| \phi_m^\lambda \right\rangle + \left\langle \phi_j^\lambda \left| \hat{n}^\lambda \right| \frac{\partial \phi_m^\lambda}{\partial t} \right\rangle. \quad (73)$$

The equation of motion for the SPFs ϕ_l^λ reads^{2,4}

$$\begin{aligned}
i \frac{\partial}{\partial t} \phi_l^\lambda &= \sum_m h_{ml}^\lambda \phi_m^\lambda \\
&+ (1 - \hat{P}^\lambda) \sum_{m,k} (\rho^\lambda)_{lm}^{-1} \langle \Psi_m^\lambda | \hat{H} | \Psi_k^\lambda \rangle \phi_k^\lambda \quad (74)
\end{aligned}$$

where h^λ denotes the gauge matrix and ρ^λ the single-particle density matrix at the respective layer. Inserting the above equation into Eq.(73) and employing Eq.(70), one finds

$$\begin{aligned}
\frac{dn_{jm}^\lambda}{dt} &= i \sum_{k,l} \langle \phi_l^\lambda | \langle \Psi_l^\lambda | \hat{H} | \Psi_k^\lambda \rangle (\rho^\lambda)_{kj}^{-1} (1 - \hat{P}^\lambda) \hat{n}^\lambda | \phi_m^\lambda \rangle \\
&- i \sum_{k,l} \langle \phi_j^\lambda | \hat{n}^\lambda (1 - \hat{P}^\lambda) (\rho^\lambda)_{mk}^{-1} \langle \Psi_k^\lambda | \hat{H} | \Psi_l^\lambda \rangle | \phi_l^\lambda \rangle \\
&+ i \sum_k (h_{kj}^\lambda)^* \langle \phi_k^\lambda | \hat{n}^\lambda | \phi_m^\lambda \rangle - i \sum_k h_{km}^\lambda \langle \phi_j^\lambda | \hat{n}^\lambda | \phi_k^\lambda \rangle \\
&= i \sum_k (h_{kn}^\lambda)^* n_{km}^\lambda - i \sum_k h_{km}^\lambda n_{jk}^\lambda \quad (75)
\end{aligned}$$

For the standard gauge $h^\lambda = 0$, which is also employed in the present work, one finally finds

$$\frac{d}{dt} \langle \phi_j^\lambda | \hat{n}^\lambda | \phi_m^\lambda \rangle = 0. \quad (76)$$

Thus, the representation of the particle number operator in the basis of SPFs does not change in time. If the initial SPFs are eigenfunctions of \hat{n}^λ , the SPFs remain eigenfunctions of \hat{n}^λ at subsequent points in time.

B. Efficient Tensor Contraction

The conservation of the local particle number can be employed to devise an approach which combines the tensor contraction used in ML-MCTDH-SQR and ML-MCTDH-oSQR schemes with the particle number based truncation scheme used in MCTDHX approaches.

The idea of the approach will be illustrated for a simple example: a system with constant particle number N described by the wavefunction representation diagrammatically depicted in Fig. 12. Each bottom layer SPF ϕ_i^λ has to show a defined local particle number n_i . Thus, the bottom layer SPFs read

$$\phi_{i;n_i}^{2;1,1} = \frac{(\hat{b}_1^\dagger)^{n_i}}{\sqrt{n_i}} |0\rangle, \quad (77)$$

$$\phi_{i;n_i}^{2;1,2} = \frac{(\hat{b}_2^\dagger)^{n_i}}{\sqrt{n_i}} |0\rangle, \quad (78)$$

$$\phi_{i;n_i}^{2;2,1} = \frac{(\hat{b}_3^\dagger)^{n_i}}{\sqrt{n_i}} |0\rangle, \quad (79)$$

$$\phi_{i;n_i}^{2;2,2} = \frac{(\hat{b}_4^\dagger)^{n_i}}{\sqrt{n_i}} |0\rangle. \quad (80)$$

Note that in addition on the notation introduced in Ref.4 here the local particle number n_i has been added as an additional subscript. The first layer SPFs are then given by

$$\phi_{k;n}^{1;1} = \sum_{\substack{i,j \\ n_i+n_j=n}} A_{k;i,j}^{(2;1)} \phi_{i;n_i}^{2;1,1} \phi_{j;n_j}^{2;1,2}, \quad (81)$$

$$\phi_{k;n}^{1;2} = \sum_{\substack{i,j \\ n_i+n_j=n}} A_{k;i,j}^{(2;2)} \phi_{i;n_i}^{2;2,1} \phi_{j;n_j}^{2;2,2}. \quad (82)$$

Here the number of coefficients $A_{i,j}^{(2;1)}$ and $A_{i,j}^{(2;2)}$ which have to be considered is reduced by the local particle number constraint. On the top layer, the resulting N particle wavefunction can be written as

$$\Psi = \sum_{\substack{i,j \\ n_i+n_j=N}} A_{i,j}^1 \phi_{i;n_i}^{1;1} \phi_{j;n_j}^{1;2}. \quad (83)$$

Again, the number of terms in the expansion is reduced by the particle number constraint.

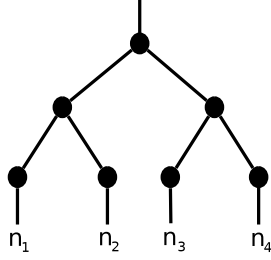


Figure 12. Diagrammatic representation of the ML-MCTDH-oSQR wavefunction discussed in Sect.VIIB.

On each layer, single hole functions $\Psi_{i;N_i}^\lambda$ with a defined local particle number N_i can be defined via

$$\Psi = \sum_i \Psi_{i;N-n_i}^\lambda \phi_{i;n_i}^\lambda. \quad (84)$$

The equations of motion for the SPFs on an arbitrary layer which originally read

$$i\dot{\phi}_{i;n_i}^\lambda = (1 - \hat{P}^\lambda) \sum_{j,k} (\rho^\lambda)_{ij}^{-1} \left\langle \Psi_{j;N_j}^\lambda \left| \hat{H} \right| \Psi_{k;N_k}^\lambda \right\rangle \phi_{k;n_k}^\lambda \quad (85)$$

can then be rewritten as

$$i\dot{\phi}_{i;n_i}^\lambda = (1 - \hat{P}^\lambda) \sum_{\substack{j,k \\ n_j=n_i}} (\rho^\lambda)_{ij}^{-1} \left\langle \Psi_{j;N_j}^\lambda \left| \hat{H} \right| \Psi_{k;N_k}^\lambda \right\rangle \phi_{k;n_k}^\lambda \quad (86)$$

due to particle number conservation. For Hamiltonians which can be written in a sum of product form the equations of motion can be further simplified. Here the Hamiltonian can be cast into the form

$$\hat{H} = \sum_k c_k \cdot \hat{\mathcal{H}}_{k;-a_k}^\lambda \cdot \hat{h}_{k;a_k}^\lambda \quad (87)$$

where the operator $\hat{h}_{k;a}^\lambda$ acts only on the orbitals contained in the SPFs $\phi_{m;n_m}^\lambda$ and increases the local particle number by a_k while $\hat{\mathcal{H}}_{k;-a}^\lambda$ acts only on the orbitals contained in the single-hole functions $\Psi_{m;N_m}^\lambda$ and decreases the particle number by a_k . The equations of motion then read

$$i\dot{\phi}_{i;n_i}^\lambda = (1 - \hat{P}^\lambda) \sum_k c_k \sum_{\substack{j,m \\ n_j=n_i \\ n_m=n_i-a_k}} (\rho^\lambda)_{ij}^{-1} \cdot \left\langle \Psi_{j;N_j}^\lambda \left| \hat{\mathcal{H}}_{k;-a_k}^\lambda \right| \Psi_{m;N_m}^\lambda \right\rangle \hat{h}_{k;a_k}^\lambda \phi_{m;n_m}^\lambda. \quad (88)$$

Thus, for each summand in the Hamiltonian only small subblocks of the single-hole matrices has to be considered and only specific subsets of the set of SPFs are coupled in the equations of motion. This significantly reduces the numerical effort required to solve the equations of motion.

VIII. CONCLUDING REMARKS

Imaginary time propagation with the recently introduced ML-MCTDH-oSQR approach was studied in the present work. The ML-MCTDH-oSQR approach combines time-dependent optimized orbitals known from MCTDHX-type approaches with general tensor contractions known from the ML-MCTDH-SQR approach. The equations of motions for imaginary time propagation are derived and differences between the real and imaginary time propagation are discussed. An important difference concerns the gauge operators which determine the rotation within the active orbital space. The gauge operators used in imaginary time propagations are anti-hermitian while the gauge-operators used in real-time propagations are hermitian. This has important consequences regarding the choice of an efficient 'gauge'. The natural gauge, which has found to be efficient and yield good result in real time propagations, scales unfavorably in imaginary time calculations and should be replaced by the newly introduced spectral gauge. The spectral gauge is designed to minimize the spectral width of the effective Hamiltonian. It shows a numerically favorable scaling in imaginary time calculations and yields computational results which for a given basis set size are at least as accurate as the ones obtained within the natural gauge.

Furthermore, the effects of particle number conservation have been studied. The MCTDH-SQR and MCTDH-oSQR approaches are Fock space methods which do not constrain the particle number by design. Considering a Bose-Hubbard model as an example of a particle number conserving system, the implications of particle number conservation on imaginary time propagation have been studied in detail. It is found that particle number conservation must be explicitly ensured to guarantee numerically stable results: during the imaginary time propagation small occupations of unphysical states can grow exponentially and finally result in convergence toward states with incorrect particle numbers. This issue can be resolved by the introduction of a penalty operator which explicitly increases the energy of states with an incorrect particle number.

Beside the conservation of the total particle number, an interesting local particle conservation in the tensor networks used in the MCTDH-oSQR and ML-MCTDH-(o)SQR approaches has been identified. In a second quantization representation, the bottom layer SPFs are represented in a particle number basis. If accordingly initialized, local particle number can be associated not only with each SPF on the bottom layer but also with any upper layer SPF. This local particle number is a constant of motion. The conservation law has significant numerical implications. On one hand, it can result in a complex dependence of the numerical results on the choice of the initially unoccupied SPFs in the (multi-layer) MCTDH-oSQR approach. On the other hand, it can be employed to design a new, more efficient tensor contraction scheme.

This new tensor contraction scheme combines the ad-

vantages of the MCTDHX and ML-MCTDH-oSQR approaches. It simultaneously uses a particle number based truncation scheme and tensor contraction to reduce the effective size of the tensor network. Furthermore, the equation of motions for the various elements in the tensor network show a favorable block structure resulting in a potentially very efficient quantum dynamics approach.

ACKNOWLEDGMENTS

The authors thank Sven Krönke and Peter Schmelcher for inspiring discussions. The authors are grateful for financial support via the FCI (Fonds der Chemischen Industrie).

APPENDIX A

Here the equations of motions in imaginary time, given in Eqs. (14),(15), are derived. To this end, the Dirac-Frenkel variational principle is employed. The variation of the wave function reads

$$\delta |\Psi\rangle = \sum_{i_1..i_f} (\delta A_{i_1..i_f}(t)) |\Phi_{i_1..i_f}(\tau)\rangle + \sum_{\mu=1}^f (\delta \hat{b}_\mu^\dagger) \hat{b}_\mu |\Psi\rangle. \quad (89)$$

The time-dependence of the wave function is given by

$$\frac{d}{d\tau} |\Psi\rangle = \sum_{i_1..i_f} \frac{dA_{i_1..i_f}}{d\tau} |\Phi_{i_1..i_f}(\tau)\rangle + \sum_{\mu=1}^f \frac{d\hat{b}_\mu^\dagger}{d\tau} \hat{b}_\mu |\Psi\rangle. \quad (90)$$

Inserting Eqs. (89) and (90), into a Dirac Frenkel variational principle in imaginary time,

$$0 = \left\langle \delta \Psi \left| \frac{d}{d\tau} + \hat{H} \right| \Psi \right\rangle, \quad (91)$$

yields

$$\begin{aligned} 0 = & \sum_{i_1..i_f} \delta A_{i_1..i_f}^* \left(\frac{dA_{i_1..i_f}}{d\tau} + \left\langle \Phi_{i_1..i_f} \left| \hat{H} + \sum_{\mu=1}^f \frac{d\hat{b}_\mu^\dagger}{d\tau} \hat{b}_\mu \right| \Psi \right\rangle \right) \\ & + \left\langle \Psi \left| \sum_{\mu=1}^f \hat{b}_\mu^\dagger (\delta \hat{b}_\mu) \left(\sum_{i_1..i_f} \frac{dA_{i_1..i_f}}{d\tau} \left| \Phi_{i_1..i_f} \right\rangle \right) \right. \right. \\ & \left. \left. + \hat{H} \left| \Psi \right\rangle + \sum_{\nu=1}^f \frac{d\hat{b}_\nu^\dagger}{d\tau} \hat{b}_\nu \left| \Psi \right\rangle \right\rangle \end{aligned} \quad (92)$$

Considering first the variation with respect to $A_{i_1..i_f}^*$, one finds

$$0 = \frac{dA_{i_1..i_f}}{d\tau} + \left\langle \Phi_{i_1..i_f} \left| \hat{H} - \sum_{\mu=1}^f \frac{d\hat{b}_\mu^\dagger}{d\tau} \hat{b}_\mu \right| \Psi \right\rangle. \quad (93)$$

In this equation $\frac{d\hat{b}_\mu^\dagger}{d\tau}$ can be replaced by $-\sum_{l=1}^F \hat{b}_l^\dagger \bar{h}_{l\mu}$ (see Eq. (17)). Here l runs from 1 to F , but $|\Psi\rangle$ contains only creators \hat{b}_ν^\dagger with index $\nu = 1, \dots, f$. Therefore l can be replaced by an index ν running from 1 to f . Thus, the time evolution of $A_{i_1..i_f}$ is given by

$$-\frac{dA_{i_1..i_f}}{d\tau} = \left\langle \Phi_{i_1..i_f} \left| \hat{H} - \sum_{\nu,\mu=1}^f \hat{b}_\nu^\dagger \bar{h}_{\nu\mu} \hat{b}_\mu \right| \Psi \right\rangle. \quad (94)$$

The equations of motions for the orbitals $c_{\mu k}$ are derived from Eq.(92) considering the variation with respect to \hat{b}_μ :

$$\begin{aligned} 0 = & \left\langle \Psi \left| \sum_{\mu=1}^f \hat{b}_\mu^\dagger (\delta \hat{b}_\mu) \left(\sum_{i_1..i_f} \frac{dA_{i_1..i_f}}{d\tau} \left| \Phi_{i_1..i_f} \right\rangle \right) \right. \right. \\ & \left. \left. + \hat{H} \left| \Psi \right\rangle + \sum_{\nu=1}^f \frac{d\hat{b}_\nu^\dagger}{d\tau} \hat{b}_\nu \left| \Psi \right\rangle \right\rangle \end{aligned} \quad (95)$$

Using

$$\delta \hat{b}_\mu = \delta c_{\mu k}^* \hat{a}_k \quad (96)$$

and Eq.(17) one finds

$$\begin{aligned} 0 = & \sum_{\mu=1}^f \sum_{k=1}^F (\delta c_{\mu k}^*) \left\langle \Psi \left| \hat{b}_\mu^\dagger \hat{a}_k \left(\sum_{i_1..i_f} \frac{dA_{i_1..i_f}}{d\tau} \left| \Phi_{i_1..i_f} \right\rangle \right) \right. \right. \\ & \left. \left. + \hat{H} \left| \Psi \right\rangle + \sum_{\nu=1}^f \sum_{l=1}^F \frac{dc_{\nu l}}{d\tau} \hat{a}_l^\dagger \hat{b}_\nu \left| \Psi \right\rangle \right\rangle \end{aligned} \quad (97)$$

Thus, the equations

$$\begin{aligned} 0 = & \left\langle \Psi \left| \hat{b}_\mu^\dagger \hat{a}_k \left(\sum_{i_1..i_f} \frac{dA_{i_1..i_f}}{d\tau} \left| \Phi_{i_1..i_f} \right\rangle \right) \right. \right. \\ & \left. \left. + \hat{H} \left| \Psi \right\rangle + \sum_{\nu=1}^f \sum_{l=1}^F \frac{dc_{\nu l}}{d\tau} \hat{a}_l^\dagger \hat{b}_\nu \left| \Psi \right\rangle \right\rangle \end{aligned} \quad (98)$$

have to be satisfied for all $\mu = 1, \dots, f$ and $k = 1, \dots, F$.

Inserting Eq. (94), the above equations can be rewritten as

$$\begin{aligned} 0 = & \left\langle \Psi \left| \hat{b}_\mu^\dagger \hat{a}_k \left(1 - \sum_{i_1..i_f} \left| \Phi_{i_1..i_f} \right\rangle \left\langle \Phi_{i_1..i_f} \right| \right) \right. \right. \\ & \left. \left. \cdot \left(\hat{H} + \sum_{\nu=1}^f \sum_{l=1}^F \frac{dc_{\nu l}}{d\tau} \hat{a}_l^\dagger \hat{b}_\nu \right) \left| \Psi \right\rangle \right\rangle \end{aligned} \quad (99)$$

At this point it is important to note that

$$\hat{P} = \sum_{i_1..i_f} |\Phi_{i_1..i_f}\rangle \langle \Phi_{i_1..i_f}| \quad (100)$$

is the projector onto a space spanned by all possible occupations of active orbitals included in the occupations number space $\{i_1, \dots, i_f\}$. If one assumes that this space is chosen sufficiently large to ensure that

$$\hat{P}\hat{b}_\nu^\dagger|\Psi\rangle = \hat{b}_\nu^\dagger|\Psi\rangle \quad (101)$$

for all $\nu = 1, \dots, f$, the equations can be further simplified. Then one finds

$$\begin{aligned} (1 - \hat{P})\hat{a}_k^\dagger\hat{b}_\mu|\Psi\rangle &= (1 - \hat{P})\sum_{l=1}^F c_{lk}^*\hat{b}_l^\dagger\hat{b}_\mu|\Psi\rangle \\ &= \sum_{l=f+1}^F c_{lk}^*\hat{b}_l^\dagger\hat{b}_\mu|\Psi\rangle \\ &= \left(\hat{a}_k^\dagger - \sum_{\lambda=1}^f c_{\lambda k}^*\hat{b}_\lambda^\dagger\right)\hat{b}_\mu|\Psi\rangle \\ &= \left(\hat{a}_k^\dagger - \sum_{\lambda=1}^f \sum_{l=1}^F c_{\lambda k}^*c_{\lambda l}\hat{a}_l^\dagger\right)\hat{b}_\mu|\Psi\rangle \\ &= \sum_{l=1}^F \left(\delta_{kl} - \sum_{\lambda=1}^f \sum_{l=1}^F c_{\lambda k}^*c_{\lambda l}\right)\hat{a}_l^\dagger\hat{b}_\mu|\Psi\rangle \end{aligned} \quad (102)$$

Inserting the above equation into Eq. (99) yields

$$\begin{aligned} 0 &= \sum_{l=1}^F \left(\delta_{kl} - \sum_{\lambda=1}^f c_{\lambda k}c_{\lambda l}^*\right) \\ &\quad \cdot \left\langle \Psi \left| \hat{b}_\mu^\dagger \hat{a}_l \left(\hat{H} + \sum_{\nu=1}^f \sum_{n=1}^F \frac{dc_{\nu n}}{d\tau} \hat{a}_n^\dagger \hat{b}_\nu \right) \right| \Psi \right\rangle. \end{aligned} \quad (103)$$

The above equation can be further simplified by commuting \hat{a}_l to the left:

$$\begin{aligned} 0 &= \sum_{l=1}^F \left(\delta_{kl} - \sum_{\nu=1}^f c_{\nu k}c_{\nu l}^*\right) \\ &\quad \cdot \left\{ \left\langle \Psi \left| \hat{b}_\mu^\dagger \left[\hat{a}_l, \hat{H} + \sum_{\lambda=1}^f \sum_{n=1}^F \frac{dc_{\lambda n}}{d\tau} \hat{a}_n^\dagger \hat{b}_\lambda \right] \right| \Psi \right\rangle \right. \\ &\quad \left. + \left\langle \Psi \left| \hat{b}_\mu^\dagger \left(\hat{H} + \sum_{\lambda=1}^f \sum_{n=1}^F \frac{dc_{\lambda n}}{d\tau} \hat{a}_n^\dagger \hat{b}_\lambda \right) \hat{a}_l \right| \Psi \right\rangle \right\} \end{aligned} \quad (104)$$

Using the relation $\sum_{l=1}^F (\delta_{kl} - \sum_{\nu=1}^f c_{\nu k}c_{\nu l}^*)\hat{a}_l|\Psi\rangle = 0$

yields

$$\begin{aligned} 0 &= \sum_{l=1}^F \left(\delta_{kl} - \sum_{\nu=1}^f c_{\nu k}c_{\nu l}^*\right) \\ &\quad \cdot \left\langle \Psi \left| \hat{b}_\mu^\dagger \left[\hat{a}_l, \hat{H} + \sum_{\lambda=1}^f \sum_{n=1}^F \frac{dc_{\lambda n}}{d\tau} \hat{a}_n^\dagger \hat{b}_\lambda \right] \right| \Psi \right\rangle \\ &= \sum_{l=1}^F \left(\delta_{kl} - \sum_{\nu=1}^f c_{\nu k}c_{\nu l}^*\right) \\ &\quad \cdot \left\langle \Psi \left| \hat{b}_\mu^\dagger [\hat{a}_l, H] + \sum_{\lambda=1}^f \frac{dc_{\lambda l}}{d\tau} \hat{b}_\mu^\dagger \hat{b}_\lambda \right| \Psi \right\rangle \end{aligned} \quad (105)$$

If the Hamiltonian \hat{H} is in normal order the all operators \hat{a}_i can be replaced by active operators \hat{b}_κ :

$$\begin{aligned} 0 &= \sum_{l=1}^F \left(\delta_{kl} - \sum_{\nu=1}^f c_{\nu k}c_{\nu l}^*\right) \\ &\quad \cdot \left\langle \Psi \left| \hat{b}_\mu^\dagger [\hat{a}_l, \hat{H}]_{\hat{a}_i = \sum_{\kappa=1}^f c_{\kappa i} \hat{b}_\kappa} + \sum_{\lambda=1}^f \frac{dc_{\lambda l}}{d\tau} \hat{b}_\mu^\dagger \hat{b}_\lambda \right| \Psi \right\rangle \end{aligned} \quad (106)$$

Applying the projector to each term, one finds

$$\begin{aligned} 0 &= \sum_{\mu=1}^f \sum_{k=1}^F (\delta_{\mu k}^*) \\ &\quad \cdot \left\{ \sum_{l=1}^F \left(\delta_{kl} - \sum_{\nu=1}^f c_{\nu k}c_{\nu l}^*\right) \left\langle \Psi \left| \hat{b}_\mu^\dagger [\hat{a}_l, \hat{H}]_{\hat{a}_i = \sum_{\kappa=1}^f c_{\kappa i} \hat{b}_\kappa} \right| \Psi \right\rangle \right. \\ &\quad \left. + \sum_{\nu=1}^f \frac{dc_{\nu k}}{d\tau} \left\langle \Psi \left| \hat{b}_\mu^\dagger \hat{b}_\nu \right| \Psi \right\rangle - \sum_{\nu=1}^f \bar{h}_{\nu\lambda} \left\langle \Psi \left| \hat{b}_\mu^\dagger \hat{b}_\lambda \right| \Psi \right\rangle \right\}. \end{aligned} \quad (107)$$

The resulting equation of motion for the orbitals $c_{\mu k}$ reads:

$$\begin{aligned} -\frac{dc_{\mu k}}{d\tau} &= \sum_{\nu=1}^f \bar{h}_{\mu\nu} c_{\nu k} + \sum_{l=1}^F \left(\delta_{kl} - \sum_{\nu=1}^f c_{\nu k}c_{\nu l}^*\right) \\ &\quad \cdot \sum_{\lambda=1}^f \rho_{\mu\lambda}^{-1} \left\langle \Psi \left| \hat{b}_\lambda^\dagger [\hat{a}_l, \hat{H}]_{\hat{a}_i = \sum_{\kappa=1}^f c_{\kappa i} \hat{b}_\kappa} \right| \Psi \right\rangle \end{aligned} \quad (108)$$

APPENDIX B

The properties of the spectral gauge can be illustrated by a simple example, the one-particle Hamiltonian

$$\hat{H} = \sum_{k,l=1}^F w_{kl} \hat{b}_k^\dagger \hat{b}_l. \quad (109)$$

For simplicity the analysis is presented in natural orbitals (see Eqs. (35)-(38)). Then the Hamiltonian reads

$$\hat{H} = \sum_{k,l=1}^F \tilde{w}_{kl} \hat{b}_k^\dagger \hat{b}_l \quad (110)$$

where

$$\tilde{w}_{rs} = \sum_{k,l=1}^F u_{kr}^* w_{kl} u_{sl} \quad (111)$$

The corresponding spectral gauge matrix is

$$\begin{aligned} \tilde{h}_{\xi\sigma}^{(spec)} &= \sum_{k,l=1}^F \tilde{w}_{kl} \frac{\langle \Psi | [\hat{b}_k^\dagger \hat{b}_l, \hat{b}_\xi^\dagger \hat{b}_\sigma] | \Psi \rangle}{\tilde{\rho}_\xi + \tilde{\rho}_\sigma + \epsilon} \\ &= \sum_{k,l=1}^F \tilde{w}_{kl} \frac{\delta_{l\sigma} \langle \hat{b}_k \Psi | \hat{b}_\xi \Psi \rangle - \delta_{k\xi} \langle \hat{b}_\sigma \Psi | \hat{b}_l \Psi \rangle}{\tilde{\rho}_\xi + \tilde{\rho}_\sigma + \epsilon}. \end{aligned} \quad (112)$$

Since $\hat{b}_k |\Psi\rangle = 0$ for $k = f + 1, \dots, F$, one finds

$$\tilde{h}_{\xi\sigma}^{(spec)} = \frac{\sum_{\mu=1}^f \tilde{w}_{\mu\sigma} \langle \hat{b}_\mu \Psi | \hat{b}_\xi \Psi \rangle - \sum_{\mu=1}^f \tilde{w}_{\xi\mu} \langle \hat{b}_\sigma \Psi | \hat{b}_\mu \Psi \rangle}{\tilde{\rho}_\xi + \tilde{\rho}_\sigma + \epsilon}. \quad (114)$$

Using Eq. (20), one arrives at

$$\tilde{h}_{\xi\sigma}^{(spec)} = \tilde{w}_{\xi\sigma} \frac{\tilde{\rho}_\xi - \tilde{\rho}_\sigma}{\tilde{\rho}_\xi + \tilde{\rho}_\sigma + \epsilon}. \quad (115)$$

The eigenstates of an one-particle operator show only one occupied natural orbital and a diagonal \tilde{w}_{kl} . Thus, $\tilde{h}_{\xi\sigma}^{(spec)}$ vanishes in the limit of a converged calculation. Furthermore, the action of $h^{(spec)}$ will ensure rotation of the orbital basis towards natural orbitals in course of the imaginary time propagation.

REFERENCES

- ¹Meyer, H.-D.; Manthe, U.; Cederbaum, L. S. *Chem. Phys. Lett.* **1990**, *165*, 73–78.
- ²Manthe, U.; Meyer, H.-D.; Cederbaum, L. S. *J. Chem. Phys.* **1992**, *97*, 3199–3213.
- ³Wang, H.; Thoss, M. *J. Chem. Phys.* **2003**, *119*, 1289–1299.
- ⁴Manthe, U. *J. Chem. Phys.* **2008**, *128*, 164116.
- ⁵Worth, G. A.; Meyer, H. D.; Koeppel, H.; Cederbaum, L. S.; Burghardt, I. *Int. Rev. Phys. Chem.* **2008**, *27*, 569–606.
- ⁶Westermann, T.; Brodbeck, R.; Rozhenko, A. B.; Schoeller, W. W.; Manthe, U. *J. Chem. Phys.* **2011**, *135*, 184102.
- ⁷Westermann, T.; Kim, J. B.; Weichman, M. L.; Hock, C.; Yacovitch, T. I.; Palma, J.; Neumark, D. M.; Manthe, U. *Angew. Chem. Int. Ed.* **2014**, *53*, 1122.
- ⁸Wilner, E. Y.; Wang, H.; Thoss, M.; Rabani, E. *Phys. Rev. B* **2014**, *89*, 205129.
- ⁹Wang, H. *J. Phys. Chem. A* **2014**, *118*, 9253–9261.
- ¹⁰Balzer, K.; Li, Z.; Vendrell, O.; Eckstein, M. *Phys. Rev. B* **2015**, *91*, 045136.
- ¹¹Schroeter, M.; Kuehn, O. *J. Phys. Chem. A* **2013**, *117*(32), 7580–7588.
- ¹²Saab, M.; Sala, M.; Lasorne, B.; Gatti, F.; Guerin, S. *J. Chem. Phys.* **2014**, *141*, 134114.
- ¹³Lopez-Lopez, S.; Martinazzo, R.; Nest, M. *J. Chem. Phys.* **2011**, *134*(9), 094102.
- ¹⁴Bouakline, F.; Lueder, F.; Martinazzo, R.; Saalfrank, P. *J. Phys. Chem. A* **2012**, *116*(46), 11118–11127.
- ¹⁵Uranga-Pina, L.; Meier, C.; Rubayo-Soneira, J. *Chem. Phys. Lett.* **2012**, *543*, 12–18.
- ¹⁶Moix Teixidor, M.; Huarte-Larranaga, F. *Chem. Phys.* **2012**, *399*, 264–271.
- ¹⁷Wahl, J.; Binder, R.; Burghardt, I. *Comp. Theo. Chem.* **2014**, *1040*, 167–176.
- ¹⁸Pflanzner, A. C.; Zoellner, S.; Schmelcher, P. *Phys. Rev. A* **2010**, *81*, 023612.
- ¹⁹Reddy, V. S.; Camacho, C.; Xia, J.; Jasti, R.; Irle, S. *J. Chem. Theo. Comp.* **2014**, *10*, 4025–4036.
- ²⁰Eisfeld, W.; Vieuxmaire, O.; Viel, A. *J. Chem. Phys.* **2014**, *140*, 224109.
- ²¹Valdes, A.; Prosimiti, R. *J. Phys. Chem. A* **2013**, *117*(39), 9518–9524.
- ²²Mondal, T.; Reddy, S. R.; Mahapatra, S. *J. Chem. Phys.* **2012**, *137*(5), 054311.
- ²³Skouteris, D.; Lagana, A. *Chem. Phys. Lett.* **2013**, *575*, 18–22.
- ²⁴Zhao, B.; Zhang, D.-H.; Lee, S.-Y.; Sun, Z. *J. Chem. Phys.* **2014**, *140*, 164108.
- ²⁵Huarte-Larrañaga, F.; Manthe, U. *J. Chem. Phys.* **2000**, *113*, 5115–5118.
- ²⁶Huarte-Larrañaga, F.; Manthe, U. *J. Phys. Chem. A* **2001**, *105*, 2522–2529.
- ²⁷Wu, T.; Werner, H.-J.; Manthe, U. *Science* **2004**, *306*, 2227–2229.
- ²⁸Schiffel, G.; Manthe, U. *J. Chem. Phys.* **2010**, *132*, 084103.
- ²⁹van Harrevelt, R.; Nyman, G.; Manthe, U. *J. Chem. Phys.* **2007**, *126*, 084303.
- ³⁰Nyman, G.; van Harrevelt, R.; Manthe, U. *J. Phys. Chem. A* **2007**, *111*, 10331–10334.
- ³¹Schiffel, G.; Manthe, U. *J. Chem. Phys.* **2010**, *132*, 191101.
- ³²Schiffel, G.; Manthe, U. *J. Chem. Phys.* **2010**, *133*, 174124.
- ³³Welsch, R.; Manthe, U. *J. Chem. Phys.* **2014**, *141*, 051102.
- ³⁴Welsch, R.; Manthe, U. *J. Chem. Phys.* **2014**, *141*, 174313.
- ³⁵Welsch, R.; Manthe, U. *J. Chem. Phys.* **2015**, *142*, 064309.
- ³⁶Welsch, R.; Manthe, U. *J. Phys. Chem. Lett.* **2015**, *6*, 338–342.
- ³⁷Ellerbrock, R.; Manthe, U. *The Journal of chemical physics* **2017**, *147*(24), 241104.
- ³⁸Ellerbrock, R.; Manthe, U. *The Journal of chemical physics* **2018**, *148*(22), 224303.
- ³⁹Coutinho-Neto, M. D.; Viel, A.; Manthe, U. *J. Chem. Phys.* **2004**, *121*, 9207–9210.
- ⁴⁰Hammer, T.; Coutinho-Neto, M. D.; Viel, A.; Manthe, U. *J. Chem. Phys.* **2009**, *131*, 224109.
- ⁴¹Hammer, T.; Manthe, U. *J. Chem. Phys.* **2011**, *134*, 224305.
- ⁴²Schroeder, M.; Gatti, F.; Meyer, H.-D. *J. Chem. Phys.* **2011**, *134*, 234307.
- ⁴³Hammer, T.; Manthe, U. *J. Chem. Phys.* **2012**, *136*, 054105.
- ⁴⁴Schroeder, M.; Meyer, H.-D. *J. Chem. Phys.* **2014**, *141*, 034116.
- ⁴⁵Vendrell, O.; Gatti, F.; Lauvergnat, D.; Meyer, H.-D. *Angew. Chemie Int. Ed.* **2007**, *46*, 6918–6921.
- ⁴⁶Vendrell, O.; Gatti, F.; Lauvergnat, D.; Meyer, H.-D. *J. Chem. Phys.* **2007**, *127*, 184302.
- ⁴⁷Vendrell, O.; Gatti, F.; Meyer, H.-D. *J. Chem. Phys.* **2007**, *127*, 184303.
- ⁴⁸Vendrell, O.; Brill, M.; Gatti, F.; Meyer, H.-D. *J. Chem. Phys.* **2009**, *130*, 234305.
- ⁴⁹Vendrell, O.; Gatti, F.; Meyer, H.-D. *J. Chem. Phys.* **2009**, *131*, 034308.

- ⁵⁰Worth, G. A.; Meyer, H.-D.; Cederbaum, L. S. *J. Chem. Phys.* **1996**, *105*, 4412–4426.
- ⁵¹Worth, G. A.; Meyer, H.-D.; Cederbaum, L. S. *J. Chem. Phys.* **1998**, *109*, 3518–3529.
- ⁵²Raab, A.; Worth, G. A.; Meyer, H.-D.; Cederbaum, L. S. *J. Chem. Phys.* **1999**, *110*, 936–946.
- ⁵³Wang, H.; Skinner, D. E.; Thoss, M. *J. Chem. Phys.* **2006**, *125*, 174502.
- ⁵⁴Wang, H.; Thoss, M. *J. Phys. Chem. A* **2007**, *111*, 10369–10375.
- ⁵⁵Kondov, I.; Cizek, M.; Benesch, C.; Thoss, M.; Wang, H. *J. Phys. Chem. C* **2007**, *111*, 11970–10981.
- ⁵⁶Craig, I. R.; Thoss, M.; Wang, H. *J. Chem. Phys.* **2011**, *135*, 064504.
- ⁵⁷Wang, H. *J. Phys. Chem. A* **2015**, *119*, 7951–7965.
- ⁵⁸Zanghellini, J.; Kitzler, M.; Fabian, C.; Brabec, T.; Scrinzi, A. *Laser Phys.* **2003**, *13*, 1064–1068.
- ⁵⁹Kato, T.; Kono, H. *Chem. Phys. Lett.* **2004**, *392*, 533–540.
- ⁶⁰Nest, M.; Klamroth, T.; Saalfrank, P. *J. Chem. Phys.* **2005**, *122*, 124102.
- ⁶¹Streltsov, A. I.; Alon, O. E.; Cederbaum, L. S. *Phys. Rev. Lett.* **2007**, *99*, 030402.
- ⁶²Alon, O. E.; Streltsov, A. I.; Cederbaum, L. S. *Phys. Rev. A* **2008**, *77*, 033613.
- ⁶³Cao, L.; Kroenke, S.; Vendrell, O.; Schmelcher, P. *J. Chem. Phys.* **2013**, *139*, 134103.
- ⁶⁴Wang, H.; Thoss, M. *J. Chem. Phys.* **2009**, *131*, 024114.
- ⁶⁵Sakmann, K.; Streltsov, A. I.; Alon, O. E.; Cederbaum, L. S. *Phys. Rev. Lett.* **2009**, *103*, 220601.
- ⁶⁶Lode, A. U. J.; Streltsov, A. I.; Sakmann, K.; Alon, O. E.; Cederbaum, L. S. *PNAS* **2012**, *109*, 13521–13525.
- ⁶⁷Mistakidis, S.; Schmelcher, P. *Physical Review A* **2017**, *95*(1), 013625.
- ⁶⁸Schurer, J.; Gerritsma, R.; Schmelcher, P.; Negretti, A. *Physical Review A* **2016**, *93*(6), 063602.
- ⁶⁹Schmitz, R.; Krönke, S.; Cao, L.; Schmelcher, P. *Physical Review A* **2013**, *88*(4), 043601.
- ⁷⁰Schmitz, R.; Krönke, S.; Cao, L.; Schmelcher, P. *Physical Review A* **2013**, *88*(4), 043601.
- ⁷¹Krönke, S.; Schmelcher, P. *Physical Review A* **2015**, *91*(5), 053614.
- ⁷²Mistakidis, S.; Cao, L.; Schmelcher, P. *Physical Review A* **2015**, *91*(3), 033611.
- ⁷³Beinke, R.; Klaiman, S.; Cederbaum, L. S.; Streltsov, A. I.; Alon, O. E. *Physical Review A* **2015**, *92*(4), 043627.
- ⁷⁴Koutentakis, G.; Mistakidis, S.; Schmelcher, P. *Physical Review A* **2017**, *95*(1), 013617.
- ⁷⁵Cao, L.; Mistakidis, S. I.; Deng, X.; Schmelcher, P. *Chemical Physics* **2017**, *482*, 303–310.
- ⁷⁶Streltsov, A. I. *Physical Review A* **2013**, *88*(4), 041602.
- ⁷⁷Fischer, U. R.; Lode, A. U.; Chatterjee, B. *Physical Review A* **2015**, *91*(6), 063621.
- ⁷⁸Krönke, S.; Knörzer, J.; Schmelcher, P. *New Journal of Physics* **2015**, *17*(5), 053001.
- ⁷⁹Chatterjee, B.; Brouzos, I.; Cao, L.; Schmelcher, P. *Physical Review A* **2012**, *85*(1), 013611.
- ⁸⁰Schurer, J.; Negretti, A.; Schmelcher, P. *Physical review letters* **2017**, *119*(6), 063001.
- ⁸¹Katsimiga, G.; Koutentakis, G.; Mistakidis, S.; Kevrekidis, P.; Schmelcher, P. *New Journal of Physics* **2017**, *19*(7), 073004.
- ⁸²Bolsinger, V.; Krönke, S.; Schmelcher, P. *Physical Review A* **2017**, *96*(1), 013618.
- ⁸³Wells, T.; Lode, A.; Bagnato, V. S.; Tsatsos, M. *Journal of Low Temperature Physics* **2015**, *180*(1-2), 133–143.
- ⁸⁴Weiner, S. E.; Tsatsos, M. C.; Cederbaum, L. S.; Lode, A. U. *Scientific reports* **2017**, *7*, 40122.
- ⁸⁵Köhler, F.; Keiler, K.; Mistakidis, S.; Meyer, H.-D.; Schmelcher, P. *arXiv preprint arXiv:1904.10358* **2019**.
- ⁸⁶Caillat, J.; Zanghellini, J.; Kitzler, M.; Koch, O.; Kreuzer, W.; Scrinzi, A. *Phys. Rev. A* **2005**, *71*, 012712.
- ⁸⁷Kato, T.; Kono, H. *J. Chem. Phys.* **2008**, *128*, 184102.
- ⁸⁸Koch, O.; Kreuzer, W.; Scrinzi, A. *Applied mathematics and computation* **2006**, *173*(2), 960–976.
- ⁸⁹Jordan, G.; Caillat, J.; Ede, C.; Scrinzi, A. *Journal of Physics B: Atomic, Molecular and Optical Physics* **2006**, *39*(13), S341.
- ⁹⁰Kitzler, M.; Zanghellini, J.; Jungreuthmayer, C.; Smits, M.; Scrinzi, A.; Brabec, T. *Phys. Rev. A* **2004**, *70*, 041401.
- ⁹¹Hochstuhl, D.; Bonitz, M. *The Journal of chemical physics* **2011**, *134*(8), 084106.
- ⁹²Li, W.; Xu, W. *Molecular Physics* **2013**, *111*(1), 119–122.
- ⁹³Zanghellini, J.; Jungreuthmayer, C.; Brabec, T. *Journal of Physics B: Atomic, Molecular and Optical Physics* **2006**, *39*(3), 709.
- ⁹⁴Nest, M. *Journal of Theoretical and Computational Chemistry* **2007**, *6*(03), 563–574.
- ⁹⁵Nest, M.; Padmanaban, R.; Saalfrank, P. *The Journal of chemical physics* **2007**, *126*(21), 214106.
- ⁹⁶Kato, T.; Yamanouchi, K. *The Journal of chemical physics* **2009**, *131*(16), 164118.
- ⁹⁷Fasshauer, E.; Lode, A. U. *Physical Review A* **2016**, *93*(3), 033635.
- ⁹⁸Ide, Y.; Kato, T.; Yamanouchi, K. *Chemical Physics Letters* **2014**, *595*, 180–184.
- ⁹⁹Alon, O. E.; Streltsov, A. I.; Cederbaum, L. S. *J. Chem. Phys.* **2007**, *127*(15), 154103.
- ¹⁰⁰Alon, O. E.; Streltsov, A. I.; Cederbaum, L. S. *Phys. Rev. A* **2007**, *76*, 062501.
- ¹⁰¹Streltsov, A. I.; Alon, O. E.; Cederbaum, L. S. *Phys. Rev. A* **2010**, *81*, 022124.
- ¹⁰²Cao, L.; Bolsinger, V.; Mistakidis, S.; Koutentakis, G.; Krönke, S.; Schurer, J.; Schmelcher, P. *The Journal of chemical physics* **2017**, *147*(4), 044106.
- ¹⁰³Wang, H.; Pshenichnyuk, I.; Härtle, R.; Thoss, M. *J. Chem. Phys.* **2011**, *135*, 244506.
- ¹⁰⁴Albrecht, K. F.; Wang, H.; Mühlbacher, L.; Thoss, M.; Komnik, A. *Phys. Rev. B* **2012**, *86*, 081412.
- ¹⁰⁵Wang, H.; Thoss, M. *J. Chem. Phys.* **2013**, *138*, 134704.
- ¹⁰⁶Wang, H.; Thoss, M. *J. Phys. Chem. A* **2013**, *117*, 7431–7441.
- ¹⁰⁷Wilner, E. Y.; Wang, H.; Thoss, M.; Rabani, E. *Phys. Rev. B* **2014**, *89*, 205129.
- ¹⁰⁸Wang, H.; Thoss, M. *Chemical Physics* **2018**, *509*, 13–19.
- ¹⁰⁹Manthe, U.; Weike, T. *J. Chem. Phys.* **2017**, *146*, 064117.
- ¹¹⁰Löwdin, P. *Phys. Rev.* **1956**, *101*, 1730–1739.
- ¹¹¹Jäckle, A.; Meyer, H.-D. *J. Chem. Phys.* **1996**, *104*, 7974–7984.
- ¹¹²Weike, T. Wellenfunktionsbasierte beschreibung der quantendynamik ununterscheidbarer teilchen Master’s thesis, Universität Bielefeld, **2017**.
- ¹¹³Beck, M. H.; Meyer, H.-D. *Z. Phys. D* **1997**, *42*, 113–129.
- ¹¹⁴Manthe, U. *Chem. Phys.* **2006**, *329*, 168–178.
- ¹¹⁵Press, W. H.; Teukolsky, S. A.; Vetterling, W. T.; Flannery, B. P. *Numerical recipes in Fortran 77: the art of scientific computing*, Vol. 2; Cambridge university press Cambridge, 1992.
- ¹¹⁶Lode, A. U.; Bruder, C. *Physical Review A* **2016**, *94*(1), 013616.
- ¹¹⁷Manthe, U. *J. Chem. Phys.* **2015**, *142*, 244109.
- ¹¹⁸Manthe, U. *Chem. Phys.* **2018**, *515*, 279–286.